

1 Strombolian eruptions and dynamics of magma degassing at Yasur 2 Volcano (Vanuatu)

3 Julia Woitischek^{1,2}, Andrew W. Woods^{1,2}, Marie Edmonds¹, Clive Oppenheimer³, Alessandro
4 Aiuppa⁴, Tom D. Pering⁵, Tehnuka Ilanko⁵, Roberto D'Aleo⁶, Esline Garaebiti⁷

5
6 ¹ Department of Earth Sciences, University of Cambridge, Downing Street, Cambridge, CB2 3 EQ,
7 United Kingdom

8 ² BP Institute, University of Cambridge, Madingley Road, Cambridge, CB3 0EZ, United Kingdom

9 ³ Department of Geography, University of Cambridge, Downing Pl, Cambridge, CB2 3EN, United
10 Kingdom

11 ⁴ Dipartimento di Scienze della Terra e del Mare (DiSTEM), Università degli Studi di Palermo, Via
12 Archirafi 36, Palermo 90123, Italy

13 ⁵ Department of Geography, University of Sheffield, Winter Street, Sheffield, S10 2TN, United
14 Kingdom

15 ⁶ INGV, Sezione di Palermo, Via Ugo la Malfa 153, 90146, Palermo, Italy

16 ⁷ Vanuatu Meteorology and Geohazards Department, Lini Highway, Port Vila, Vanuatu

17 18 Highlights:

- 19 • FTIR and MultiGAS measurements at Yasur Volcano constrain volcanic gas
20 compositions
- 21 • A new model is proposed to explain the cyclic variation in gas geochemistry, based
22 on rupture and reforming of a crystal-rich plug.
- 23 • High fluxes of volcanic gases have persisted at Yasur Volcano for decades.
24

25 Abstract

26 Open vent basaltic volcanoes account for a substantial portion of the global atmospheric
27 outgassing flux, largely through passive degassing and mild explosive activity. We present
28 volcanic gas flux and composition data from Yasur Volcano, Vanuatu collected in July 2018.
29 The average volcanic plume chemistry is characterised by a mean molar CO₂/SO₂ ratio of
30 2.14, H₂O/SO₂ of 148 and SO₂/HCl of 1.02. The measured mean SO₂ flux on 8 July is 4.2 kg
31 s⁻¹. Therefore, the mean fluxes of the other species are 5.9 kg·s⁻¹ CO₂, 224 kg·s⁻¹ H₂O and 2.3
32 kg·s⁻¹ HCl. The degassing regime at Yasur volcano ranges from 'passive' to 'active' styles,
33 with the latter including Strombolian activity and spattering. Gases emitted during active
34 degassing are enriched in SO₂ over HCl and CO₂ over SO₂ relative to passive degassing, with
35 CO₂/SO₂ ratios of 2.85 ± 0.17, SO₂/HCl of 1.7 ± 0.22, and H₂O/SO₂ of 315 ± 78.8. Gases
36 emitted during passive degassing have CO₂/SO₂ ratios of 1.96 ± 0.12, SO₂/HCl of 0.50 ± 0.07

37 and H₂O/SO₂ of 174 ± 43.5 . We use a model of volatile degassing derived from melt
38 inclusion studies (Metrich et al., 2011), combined with our observations of chemical
39 variations in the outgassing bubbles to propose a mechanism for magma degassing in the
40 conduit at Yasur. We envisage a shallow conduit filled with crystal-rich magma, forming a
41 viscous and mobile plug that develops an effective yield strength from the surface to a depth
42 of at least 1600 m, in which bubbles are trapped, grow, ascend towards the surface and burst
43 in a typical Strombolian eruption. Deeper bubbles released during active degassing are
44 enriched in CO₂ and SO₂ compared to bubbles released during ‘passive degassing’, which are
45 sourced from close to the surface, and are, consequently, HCl-rich.

46

47 Keywords: basaltic open vent volcanoes, Strombolian activity, Yasur, crystal content in
48 magma, gas fluxes, magma fluxes.

49

50 **1. Introduction**

51 Basaltic volcanoes contribute a large proportion of the volcanic gas flux to the atmosphere
52 (Burton et al., 2013, Aiuppa et al., 2019). Six of the ten most prolific volcanic outgassers are
53 basaltic open-vent volcanoes (Burton et al., 2013, Carn et al., 2017), wherein degassing takes
54 place from the free magma surface at an open vent. Characterising this style of degassing is
55 important in order to monitor volcanic hazard, understand their role in the geochemical
56 cycling of volatiles between the interior and atmosphere on a planetary scale, and quantify
57 the volumes and depths of the magma bodies responsible for driving the degassing. The
58 activity observed at basaltic open-vent volcanoes is characterised by a range of degassing
59 regimes, from passive degassing and lava lake activity, through Strombolian activity, lava
60 fountaining and sub-Plinian eruptions (e.g. Blackburn et al, 1976, Williams, 1983, Walker et
61 al., 1984, Coltelli et al., 1995, Allard et al., 2005, Burton et al., 2007a, Aiuppa et al., 2010,
62 Ilyinskaya et al., 2012, Tamburello et al., 2012). These styles of activity are dependent, to
63 varying degrees, on magma rise speed, magma volatile content, bubble-melt separation depth,
64 bubble ascent velocity and bulk magma viscosity (Wilson and Head, 1981, 1983, Parfitt and
65 Wilson, 1995, Slezin, 2003, Houghton and Gonnerman, 2008).

66

67 Strombolian activity is associated with the bursting of large bubbles termed gas slugs (or
68 Taylor bubbles) at the vent or lava lake surface (Blackburn et al., 1976, Sparks, 1978, Burton
69 et al., 2007a, Houghton and Gonnermann, 2008, Parfitt, E.A., 2004, Pering et al., 2015). It is
70 common at basaltic volcanoes because the comparatively low viscosity of the melt ($10 - 10^4$

71 Pa·s) allows gas-melt segregation and bubble coalescence processes on the timescale of
72 magma rise (Batchelor, 1967, Jaupart and Vergnolle, 1988, 1989, Woods and Cardoso, 1997,
73 Francis and Oppenheimer, 2004, Parfitt and Wilson, 2008, James et al., 2009,). Gas slugs can
74 range in length up to 200 m (Taddeucci et al., 2010, Del Bello et al., 2012,). The rise of a
75 large gas bubble or slug is often accompanied by an increase in the height of the magma
76 surface until the bubble bursts at the surface and releases a large volume of magmatic gas,
77 ejecting metre-scale molten magma fragments and ash into the air (Taddeucci et al., 2012a,b,
78 Gaudin et al., 2016, Houghton et al., 2008). Typical volumes of gas released by a single
79 bubble at Stromboli vary from 10 – 1000 m³ (Vergnolle and Brandeis, 1996, Ripepe and
80 Marchetti, 2002, Mori and Burton, 2009, Del Bello et al., 2012, Pering and McGonigle,
81 2018). Another key characteristic of Strombolian eruptions is periodic or quasi-periodic,
82 short-duration eruptions (5-6 events of 5-10 seconds duration per hour) (Allard et al., 1994,
83 Ripepe and Harris., 2008, Taddeucci et al., 2012a,b, Houghton et al., 2016, Gaudin et al.,
84 2016).

85
86 Among the volcanoes that exhibit strombolian behaviour are Stromboli (Italy), Pacaya
87 (Guatemala), Erebus (Antarctica), Villarrica (Chile), Reventador (Ecuador), Arenal (Costa
88 Rica) and Yasur (Vanuatu) (Ntepe and Dorel, 1990, Neuberg et al., 1994, Vergnolle and
89 Brandeis, 1996, Seyfried and Hort, 1999, Chouet et al., 1999,2003, Urbanski et al., 2002,
90 Hort et al., 2003, Oppenheimer et al., 2006, Ripepe et al., 2007; Patrick et al., 2007, Gaudin
91 et al., 2014, Ripepe et al., 1993). Strombolian activity is characterised by discrete, rhythmic,
92 mild to moderate bursting of over-pressurised bubbles lasting for a few seconds, with a low
93 eruption rate of a variety of pyroclastics including lapilli, bombs, ash and lithic blocks (Rosi
94 et al., 2013, Houghton et al., 2016). This typical activity can be subdivided qualitatively into
95 normal, major and paroxysmal kinds of explosion (Rosi et al., 2013) or, based on the
96 products of the explosion, into ballistic- or ash-dominated explosions (Rosi et al., 2013,
97 Patrick et al., 2007, Gaudin et al., 2017). The transition between these different types of
98 eruption is still not well understood but might correlate with the slug size and the presence of
99 a layer of degassed and cooled magma on top (Del Bello et al., 2015, Capponi et al., 2016,
100 Spina et al., 2019b, Oppenheimer et al., 2020)

101
102 Between strombolian eruptions, many open vent basaltic volcanoes exhibit persistent
103 degassing (Andres and Kasgnoc, 1998, Aiuppa et al., 2008, Burton et al., 2000, Burton et al.,

104 2013, Carn et al., 2017, Girona et al., 2015.), which is poorly understood. Persistent
105 degassing has been linked to magma convection in the conduit, whereby gas-rich magma
106 rises and outgasses, then denser, gas-poor magma sinks back down the conduit, supplying gas
107 to the atmosphere without eruption of magma (Francis et al., 1993, Allard et al., 1994,
108 Kazahaya et al., 1994, Stevenson and Blake 1998, Burton et al., 2007b, Huppert and
109 Hallworth., 2007, Beckett et al., 2014). The rate of magma convection for Stromboli, for
110 example, has been proposed to range from 300-1300 kg·s⁻¹ (Harris and Stevenson, 1997), to
111 account for the flux of magmatic gases emitted from the volcano (Allard et al., 1994). The
112 style of magma flow in the conduit may be described either as Poiseuille flow (steady,
113 axisymmetric flow through a pipe) or, if the conduit is inclined, bubbly magma will ascend
114 along the upper wall and degassed magma back down along the lower wall (James et al.,
115 2004); or as the ascent of undegassed magma spheres through stagnant, degassed magma
116 (Koyaguchi, 1985, 1987, Kazahaya et al., 1994). In order to sustain surface degassing
117 continuously for long timescales (e.g. over 10³ years at Stromboli Volcano), a continuous
118 input of new volatile-rich magma is required to be supplied to the shallow plumbing system
119 (Francis et al., 1993; Allard et al., 2005, Burton et al., 2007b, Girona et al., 2015.).

120 Typical models of magma convection in a conduit are simplified models of two-phase
121 exchange flows, in which melt is assumed to rise to a specific depth, degas and then return to
122 a deeper reservoir. In practice, convection processes will be more complex due to
123 crystallisation and the exsolution of gas from melt during magma ascent. An increase in
124 magma crystallinity can dramatically affect the rheological properties of the ascending
125 magma and therefore, also influence eruption style (Sparks, 1978, Belien et al., 2010,
126 Cimarelli, et al., 2011, Oppenheimer et al., 2015, Barth et al., 2019). The presence of a
127 crystal phase in a liquid may strongly influence the mobility of bubbles, as shown in recent
128 studies involving three-phase analogue experiments (Belien et al., 2010; Oppenheimer et al.,
129 2015, 2020, Barth et al., 2019). In a densely packed suspension, outgassing occurs as bursts
130 or puffs because the granular network in the particle pack resists bubble growth and instead
131 promotes bubble coalescence and the formation of permeable pathways (Oppenheimer et al.
132 2015). Similar experimental results were presented by Barth et al. (2019), who proposed that
133 the episodic gas release during Strombolian eruptions occurs because crystalline mush in the
134 shallow plumbing system acts as a valve to control a continuous gas supply. In their model,
135 the size of the gas pocket depends on the overpressure within the bubble prior to the tensile
136 failure of the particle-rich suspension. These experiments provide new insights into the

137 mechanisms linking degassing cyclicality to the presence of crystals. Numerical simulations
138 performed by Parmigiani et al., (2014, 2016, 2017) focusses on the interaction between
139 bubbles and crystals at a pore scale. In their simulations, bubbles accumulate in the magma
140 until they overcome the capillary pressure within the pores in the crystalline magma, which
141 promotes bubble coalescence. Additionally, the authors propose that the bubble transport
142 dynamics changes with increasing crystal volume fraction: from suspension and channel
143 formation to the arrest of bubbles. In analogue experiments, Pistone et al., (2017) observed
144 that at high crystal fractions, gas exsolution can generate sufficient overpressure to form
145 microfractures in the magma. Spina et al, (2019 b) illustrated the strong control of
146 crystallinity on gas permeability and mobility in analogue magmas in a series of experiments.

147 Yasur magmas typically contain > 30 vol. % crystals (Metrich et al., 2011) and thus is an
148 ideal natural laboratory to study the effect of the crystal phase on degassing dynamics. In this
149 paper, we present the results of a field campaign to measure the flux and composition of
150 volcanic gases emitted from Yasur Volcano (Vanuatu) in July 2018. We quantify gas
151 chemistry and flux changes over timescales of seconds during small-scale strombolian
152 activity, passive degassing, and recharge periods, and relate the gas composition and flux to
153 degassing mechanisms (e.g. ‘open’ vs ‘closed’ degassing and depth of gas-melt decoupling).
154 We analyse high frequency time-series of Yasur’s emitted plume composition and flux
155 collected by open-path Fourier transformed infrared spectrometer (OP-FTIR),
156 multicomponent volcanic gas analyser (MultiGAS) and ultraviolet cameras (UV cameras).
157 We also correlate several hours of video footage with the corresponding gas data to elucidate
158 differences in gas composition associated with explosion and outgassing dynamics. This
159 footage was used to document morphological changes in the crater and to count the
160 frequency of bubble bursts. We use a previously published degassing model based on melt
161 inclusion data (Metrich et al., 2011) to reconstruct volatile partitioning into an exsolved phase
162 during magma ascent from 200 MPa to the surface, and incorporate the effect of
163 crystallization in the shallow conduit. We use the observed CO₂/SO₂ ratio combined with
164 melt inclusion systematics to infer the primary minimum melt CO₂ content of the Yasur
165 melts. These model results are compared with our surface gas measurements to infer the
166 mixing (coalescence) processes and approximate depths of gas-melt separation for different
167 modes of outgassing with the aim to better understand Yasur’s shallow plumbing system. We
168 consider whether the high crystallinity of Yasur’s magma influences the outgassing style.

169 2. Geological setting

170 Mount Yasur Volcano (361 m a.s.l) is a basaltic-andesitic volcano on Tanna island, in the
171 archipelago of Vanuatu in the Southwest Pacific Ocean (**figure 1**). Tanna is located in the
172 central part of the New Hebrides Island Arc and approximately 150 km above the Benioff
173 zone caused by the subduction of the Indo-Australian underneath the Pacific plate (Carney
174 and Macfarlane, 1979; Louat et al., 1988, Bani and Lardy, 2007, Spina et al., 2016,). The
175 convergence rate varies from 90-120 mm per year and is controlled by the dynamics of the
176 subduction zone and the back-arc North-Fiji basin (Taylor et al., 1995, Vergniolle and
177 Metrich, 2016). Yasur has two summit craters, named North and South crater. Previous
178 studies refer to three active vents (A, B, C) (e.g. Bani et al., 2013) but locals reported the
179 permanent existence of four vents named Kraesun (South Crater, vent B in Bani et al., 2013),
180 Wei Wei (South Crater, vent A in Bani et al., 2013), Kaunaung (North Crater, vent C in Bani
181 et al., 2013) and Kasmiren (North Crater, vent C in Bani et al., 2013). The volcano exhibits
182 long-lived, persistent degassing, which may have been maintained over the last 1400 years
183 (Metrich et al., 2011, Vergniolle and Metrich, 2016), with sporadic Strombolian activity
184 (Oppenheimer et al., 2006, Bani et al., 2013, Gaudin et al., 2014, Battaglia et al., 2016,
185 Vergniolle and Metrich, 2016).

186
187 Previous studies of volcanic outgassing at Yasur combined a high-speed thermal camera with
188 an infrasonic sensor (Spina et al., 2016) and distinguished between two explosion classes in
189 the South crater based on distinct spectral features and waveforms: minor explosions caused
190 by small and continuously-bursting over-pressurised gas bubbles; and larger events,
191 characterized as Strombolian eruptions. According to Spina et al. (2016), these kinds of
192 eruptive events are decoupled and represent distinct mechanisms of degassing. Another
193 classification of Yasur's explosions in both North and South crater (Meier et al., 2016) based
194 on a multi-parametric dataset of doppler radar, infrared imagery, and infrasound, categorised
195 two explosion styles: ash-rich, and ash-free. A classification based solely on infrared thermal
196 imaging in the South crater (Bani et al., 2013) differentiates between low and high energy
197 events, and suggests that low-energy events originate in the shallow conduit, whereas the
198 high energy events originate deeper and are associated with the bursting of slugs. Seismic
199 (LP events) reveal that Strombolian activity is associated with signals originating at 700 –
200 1200 m below the summit (Battaglia et al., 2016). Oppenheimer et al (2006) identified, using
201 OP-FTIR measurements, variations in the SO₂/HCl molar ratio between 'passive' (degassing

202 between explosions) and ‘active’ degassing (Strombolian eruptions) in the South crater.
203 Gases emitted during Strombolian explosions at Yasur in 2005 were characterised by molar
204 SO_2/HCl ratios of up to 30 whereas those associated with passive degassing had a typical
205 ratio between about 1.5 and 2.5 (Oppenheimer et al., 2006). The differences in the SO_2/HCl
206 ratio were explained using two gas sources: a gas rich in SO_2 , sourced at a greater depth
207 where larger gas slugs are formed, and the shallower source rich in HCl and responsible for
208 passive degassing (Oppenheimer et al., 2006).

209

210 Studies quantifying the volatile contents of melt inclusions (H_2O , CO_2 , S, Cl) combined with
211 MELTS modelling (Ghiorso and Sack, 1995) have suggested that extensive degassing of the
212 melt begins at 4 or 5 km beneath the surface at Yasur (Metrich et al., 2011). In this part of the
213 plumbing system, the basaltic-trachyandesitic magma crystallizes extensively (by > 30 vol.
214 %), predominantly forming plagioclase feldspar (Metrich et al., 2011).

215

216 Ground-based gas measurements in October 2007 revealed that Yasur was emitting > 155
217 $\text{kg}\cdot\text{s}^{-1}$ H_2O , $7.9 \text{ kg}\cdot\text{s}^{-1}$ of SO_2 , $9.7 \text{ kg}\cdot\text{s}^{-1}$ CO_2 , $1.9 \text{ kg}\cdot\text{s}^{-1}$ HCl and $0.3 \text{ kg}\cdot\text{s}^{-1}$ HF (Metrich et al.,
218 2011). The SO_2 emission rate derived from satellite-based Ozone Mapping Instrument (OMI)
219 measurements from 2000 to 2015 averaged $16.3 \text{ kg}\cdot\text{s}^{-1}$ (Carn et al., 2017). As a result, Yasur
220 ranks at number 11 in a list of 91 degassing volcanic SO_2 sources (Carn et al., 2017). SO_2
221 flux measurements during field campaigns in 2004, 2005 and 2007 reveals fluxes ranging
222 from 1.9 to $14.5 \text{ kg}\cdot\text{s}^{-1}$ SO_2 in 2004 and 2005 (Bani and Lardi, 2007) and $7.9 \pm 3.8 \text{ kg}\cdot\text{s}^{-1}$ SO_2
223 in 2007 (Metrich et al., 2011).

224 3. Methods

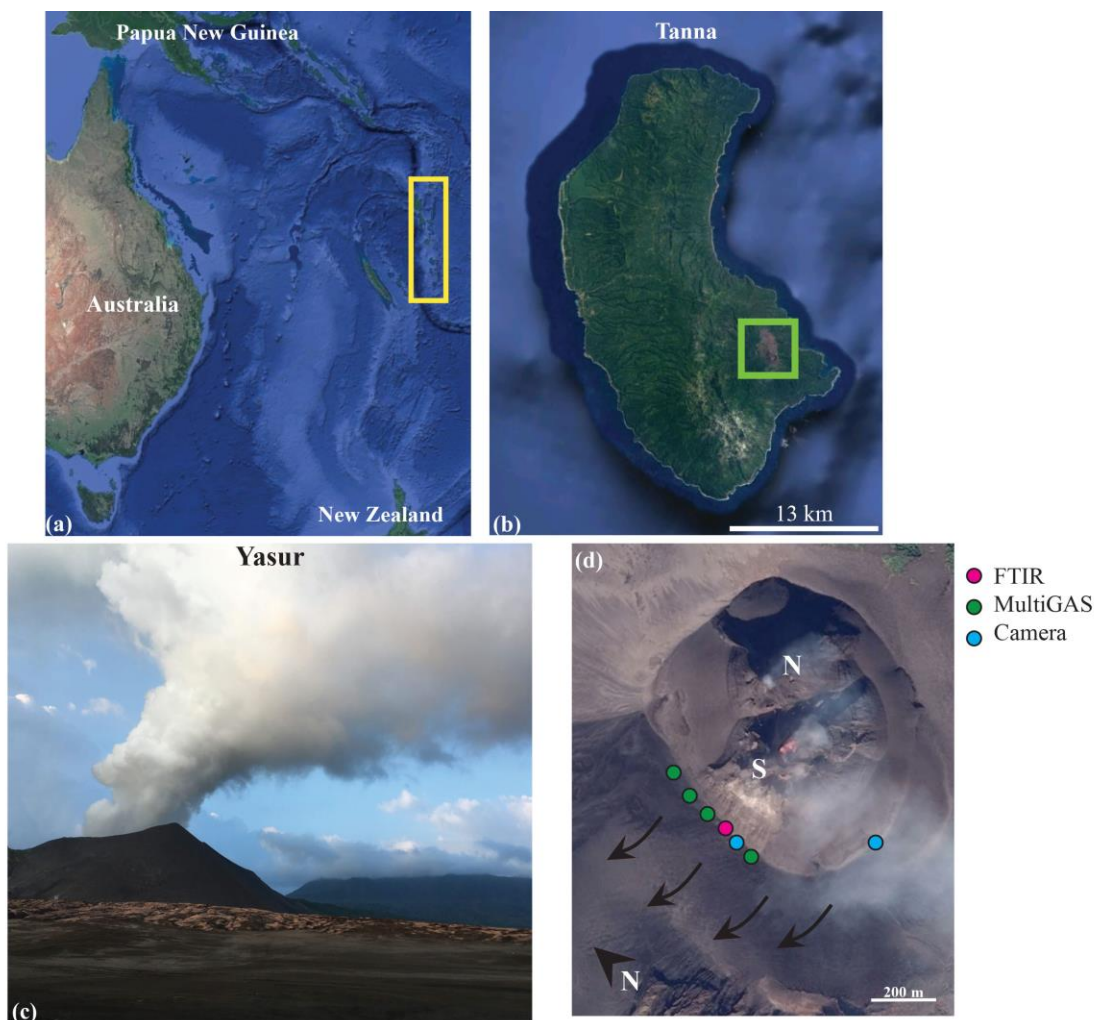
225 Volcanic gas composition and flux measurements were carried out on Yasur Volcano from 6
226 to 16 July 2018 using an open path Fourier transform infrared spectrometer (OP-FTIR),
227 Multi-GAS and UV cameras (**figure 1**). On 16 July, a MIDAC M4410-S FTIR spectrometer
228 fitted with a ZnSe beam splitter and a Stirling engine-cooled detector was deployed on the
229 southern crater rim (location shown on **figure 1e**), powered by a 20 Ah battery. A laptop
230 running AutoQuant Pro 4.5 software, connected to the FTIR, controlled data acquisition. The
231 spectrometer was placed on a tripod and positioned to collect infrared radiation from a hot
232 vent in the South crater (**figure 1**). The nominal field of view of the spectrometer is 20 mrad.
233 The distance between the infrared source and the spectrometer was approximately 300 m.

234 The volcanic gases from the multiple different vents mixed inside the crater, such that
235 measurements of gases from only one particular vent was not possible. Analysis of FTIR
236 spectra is based on the principles of absorption spectroscopy. We used the HITRAN database
237 2008, which provides the absorption coefficients (Rothman et al., 2009).

238 Spectra were acquired during the following intervals (in GMT time): 06:41-06:56 h (set 1),
239 08:19-08:24 h (set 2) and 08:56-09:03 (set 3). All interferograms were collected at a time step
240 of 1 second and a nominal 0.5 cm^{-1} spectral resolution. In total 698 spectra were collected.
241 Column amounts of SO_2 , and HCl were retrieved from single beam spectra using a code that
242 simulates and fits atmospheric transmittance in discrete wavebands (Burton et al., 2000). The
243 code gives for each selected gas a ‘goodness of fit’, which provide information about how
244 close the computed and the measured spectra fit. The average fitting error for SO_2 is 4.8 %
245 (standard deviation of the average error, sd: $\pm 0.63 \%$) and 6.9 % (sd: $\pm 0.86 \%$) for HCl.
246 Laboratory experiments were carried out in previous studies to validate the precision of the
247 measurements using primary gas standards, suggesting accuracies of order of 5 % for
248 retrieved column amounts of SO_2 and CO (Horrocks et al., 2001.). The wavebands selected to
249 retrieve volcanic gas species were: 2020 to 2100 cm^{-1} for H_2O and CO_2 , 2430 to 2530 cm^{-1}
250 for SO_2 and 2680 to 2835 cm^{-1} for HCl. The uncertainty on FTIR gas ratios was calculated by
251 propagating the errors on individual retrievals i.e. the root of the sum of the individual
252 maximum fitting errors. The maximum fitting error for SO_2 was of 8.7 % and for HCl is was
253 of 10.4 %. Therefore, the calculated error for this SO_2/HCl ratio is 14 %.

254 A multicomponent gas analyser system (MultiGAS; Aiuppa et al., 2005, 2010, Shinohara,
255 2005) was used to measure the composition of the volcanic plume (sourced from both, the
256 North and South crater; **figure 1e**) from 6 to 16 July 2018. The Multi-GAS hosts infrared
257 sensors (LI-840 NDIR closed-path spectrometer, measurement range 0-3000 ppmv for CO_2
258 accuracy, $\pm 1.5 \%$), and electrochemical sensors (model 3ST/F, Cod.TD2D-1A, City
259 Technology Ltd., calibration range, 0–30 ppmv; repeatability 1%) for SO_2 . The infrared and
260 the electrochemical sensors are protected by a pelican case and the volcanic plume is pumped
261 at a rate of 0.6 L min^{-1} to the sensors. The sensors are connected to a data logger that is
262 programmed to capture measurements of the plume at a sampling rate of 1 Hz (Aiuppa et al.,
263 2010). The Multi-GAS was placed at the southern and western rim of Yasur (**figure 1e**) and
264 powered by lithium battery. It measured the concentration of the volcanic gases by
265 integrating the infrared sensor for CO_2 , the electrochemical sensors for SO_2 and temperature,

266 pressure and relative humidity of H₂O. MultiGAS time series were post-processed by using
 267 the Ratiocalc software (Tamburello et al., 2015). Uncertainties in derived molar ratios, based
 268 on laboratory test results are, for CO₂/SO₂ with SO₂ > 0.16 mol, ± 6 % and with SO₂ < 0.16
 269 mol the error increases to ± 12% (Liu et al., 2019). Errors for H₂O/SO₂ ratios, based on
 270 laboratory tests, are ± 25%. For this study, we obtained 7523 measurements.



271
 272

273 **Figure 1** (a) Location of Vanuatu in the southwestern Pacific (yellow rectangle) (b) Tanna island
 274 with Yasur located in the eastern part of the island (green rectangle), (c) Yasur Volcano, one of
 275 the most active volcanoes in Vanuatu and the world, (d) bird's eye view of North (N) and South
 276 (S) crater of Yasur with the position of the equipment along the crater rim pointing into the South
 277 crater: FTIR (red circle), MultiGAS (green circle) and cameras (blue circle). The arrows pointing
 278 in the west showing the prevailing plume direction.
 279

280 Ultraviolet (UV) cameras (PiCam; Wilkes et al., 2017) were used to measure the emission
 281 rate of SO₂ during the same time period (the methods and results are described and presented
 282 in). The method is based on the characteristic absorption of scattered UV sunlight by SO₂
 283 between 300 and 320 nm (Mori and Burton, 2006, Kantzas et al., 2010, Kern et al., 2015).

284 The PiCam UV camera uses two UV bandpass filters that transmit radiation at about 310 nm
285 (with absorption due to SO₂) and at 330 nm (with no absorption due to SO₂). The estimated
286 error for this PiCam system is about 15% (Wilkes et al., 2017). SO₂ emission rates derived
287 from the PiCam data on 8 July 2018 were used to derive fluxes of the other gas species. The
288 calculated error for the HCl flux is 20% based on propagating errors from the SO₂ flux
289 measurement and error on molar SO₂/HCl (from FTIR).

290

291 Lastly, videos and photos captured eruptive activity enabling recording of gas burst
292 frequency, changes in crater morphology and volcanological features of the crater and vents
293 during the period of the field work, using a 12 MP camera at 60 fps (iphone SE). To compare
294 the activity between the North and South craters, a 12 MP camera at 240 fps (go pro hero 7)
295 was installed at the eastern rim to overlook the North and South craters. Both camera
296 positions in figure 1c were used to acquire video images for counting bubble bursts.

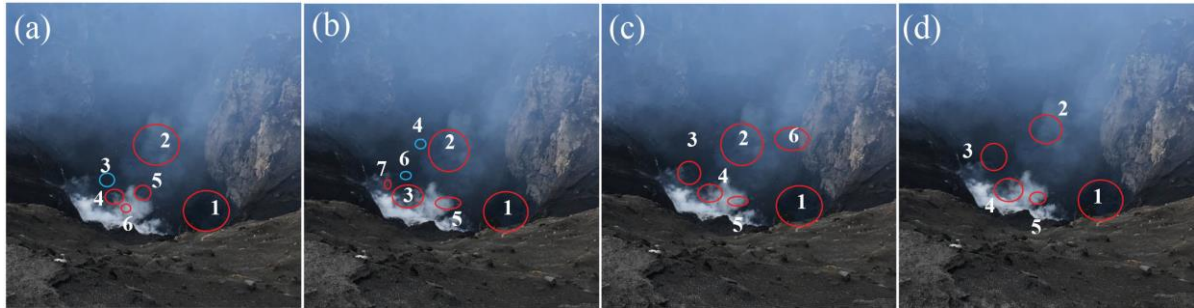
297

298 **4. Results**

299 *4.1 Video observations of the South crater*

300 The number of active vents in the South crater emitting gas and/or magma during the
301 fieldwork varied from 5 to 7 (figure 2). Six vents were observed on 9 July (figure 2a), 7 on 11
302 July (figure 2b), 6 on 13 July (figure 2c) and 5 on 15 and 16 July (figure 2d). The two
303 principal vents (vent 1 and 2 in figure 2) did not change their position during the field period
304 whereas other minor vents changed their positions and sizes or appeared and disappeared
305 from day to day. Video observations reveal that small bubble bursts generated ejecta that rose
306 a few tens of metres above the vents whereas larger bubble-bursting events generated bombs
307 that were expelled to a height of > 10 metres above the vents and landed outside the crater.
308 The overall number of large bubble bursts which were counted on the video (and generated
309 ejecta) per second was $4 \pm 0.1 \text{ s}^{-1}$ on 9 July, $1.3 \pm 0.3 \text{ s}^{-1}$ on 11 July, $0.8 \pm 0.3 \text{ s}^{-1}$ for 13 July
310 in the morning and $0.7 \pm 0.3 \text{ s}^{-1}$ in the evening and $1.3 \pm 0.1 \text{ s}^{-1}$ for 15 and 16 July. Table 1
311 shows the overall number of bubbles which were observed in different vents of figure 2. The
312 average time interval between large bubble bursts (strombolian explosions) from 8 to 16 July
313 was $54 (\pm 44)$ seconds i.e. 0.02 large bubble bursts s^{-1} . One of the principal vents exhibited a
314 consistent style of volcanic activity throughout the measurement period, characterised by
315 strombolian explosions, which expelled volcanic bombs that occasionally reached the crater

316 rim and were sometimes accompanied by shock waves. The second principal vent showed a
 317 different behaviour, exhibiting jet-like gas emission after the bursts that lasted for several
 318 seconds. These strombolian explosions ejected volcanic bombs several hundred meters into
 319 the air and were accompanied by shock waves. All the other vents were less active, erupting
 320 only a little material (via spattering).



321

322 **Figure 2** Vent location in the crater of Yasur Volcano, Vanuatu, on (a) 9th July, (b) 11th July, (c) 13th
 323 July and (d) 15th - 16th July 2018. ~Estimated field of view is between 200 and 300 m.

324

325 *Table 1. Calculated bubble bursts per s⁻¹ from vents at Yasur Volcano, Vanuatu in July 2018. The*
 326 *location of the vents are shown in figure 2 over different days. Each calculation is based on 224 to*
 327 *776 seconds worth of video data.*

day	Bubble bursts per second						
	Vent 1	Vent 2	Vent 3	Vent 4	Vent 5	Vent 6	Vent 7
9 th July	0.01	0.05		0.06	0.02		
11 th July	0.009	0.03	0.40		0.29		0.018
13 th July	0.003	0.17	0.43	0.16	0.45	0.01	
15 th /16 th July	0.009	0.36	0.26	0.26	0.36		

328

329 4.2 Volcanic plume composition from MultiGAS

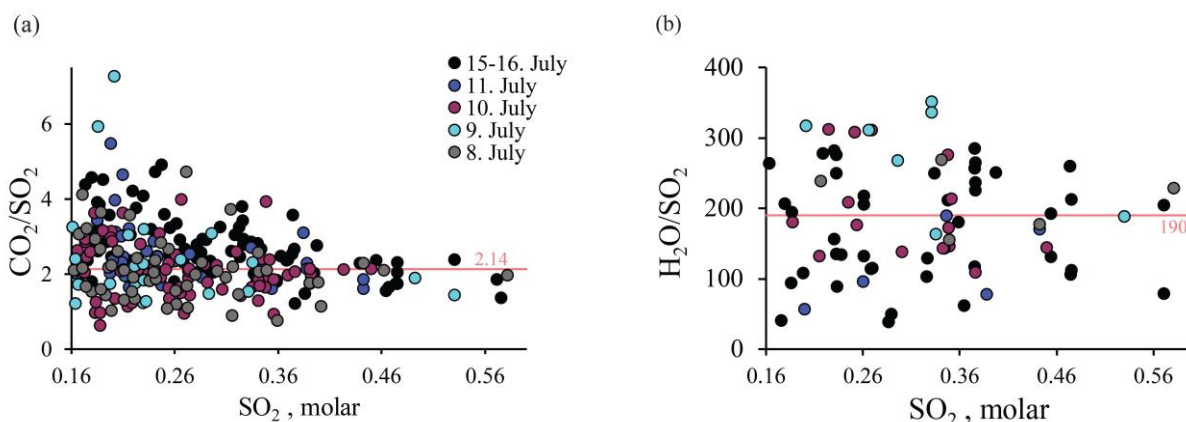
330 MultiGAS results are shown in **figure 3** and **table 2**. Across all days, the mean gas
 331 concentrations varied between 17.7 and 25.4 ppm CO₂, 14.1 to 14.8 ppm SO₂ and 364 to 854
 332 ppm H₂O. The mean volcanic gas concentrations in the plume across all four days is: 22.2
 333 ppm CO₂, 14.4 ppm SO₂ and 610 ppm H₂O. The mean molar plume composition for all four
 334 days is 97.9 mol % H₂O, 1.44 mol % CO₂ and 0.66 mol % SO₂.

335

336

337

338
339
340



341
342

343 **Figure 3** Scatter plots of Yasur Volcano's plume gas emissions for 8th to 16th July: (a) Molar
344 CO₂/SO₂ vs. SO₂ and (b) Molar H₂O/SO₂ vs. SO₂, with the average value of CO₂/SO₂ and
345 H₂O/SO₂ ratios (with SO₂>0.3) marked as a horizontal line, marked with value. Each point
346 corresponds in (a) to a CO₂/SO₂ and in (b) to a H₂O/SO₂ peak in the measured data set (CO₂/SO₂:
347 315 data points, H₂O/SO₂: 86 data points). Below SO₂ concentrations of 0.16 mol% the error
348 increases from ± 6 to ± 12%.
349

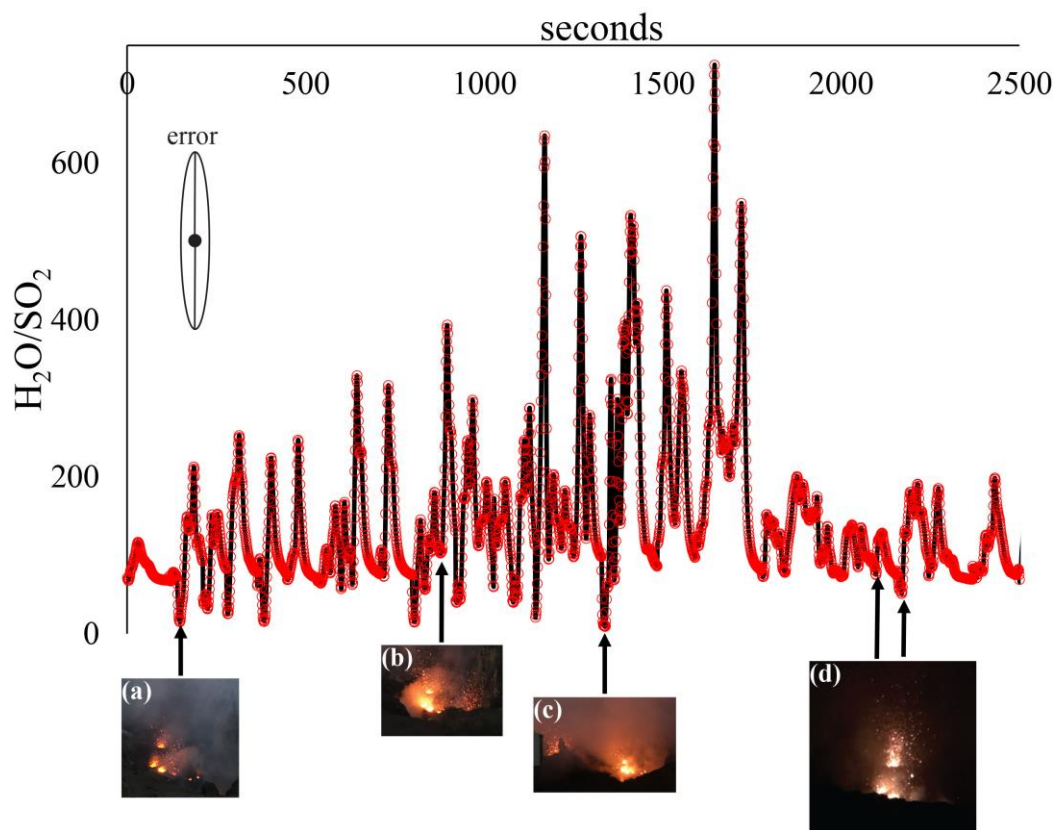
350 **Table 2** shows the mean molar CO₂/SO₂ plume ratios for all days, which ranged from 1.80
351 on 9 July to 2.48 on 16 July. **Figure 3a** shows CO₂/SO₂ ratios plotted against SO₂ for single
352 eruption gas peaks recorded in the volcanic plume for each day and shows that CO₂/SO₂ were
353 consistent from day to day, converging on an overall mean of 2.14 for molar SO₂ values >
354 0.16 (there is a larger spread at lower SO₂ values; **figure 3a**). The daily molar H₂O/SO₂
355 plume ratios (**table 2; figure 3b**) are highly variable, ranging from a mean of 89.3 ± 22.3 for
356 11 July and 205 ± 51.3 for 16 July with a mean value of 190 for molar SO₂ values > 0.3 mol
357 %, although there is considerable scatter (**figure 3b**). This variability in molar H₂O/SO₂ is
358 linked strongly to degassing regime: low H₂O/SO₂ is associated with powerful strombolian
359 eruptions (**figure 2a-d**).

360 *Table 2: Composition of Yasur Volcano's volcanic gas plume measured by MultiGAS on for 9, 10, 11,*
361 *and 16 July 2018. n: number of measurements including data measurements with SO₂ < 0.16 mol,*
362 **mean concentration, in ppm (standard deviation), ^smolar percentage of each component, [^]molar*
363 *ratios.*

		16 July	11 July	10 July	9 July	Mean
	<i>n</i>	4809	959	1280	475	
*Mean concentration	CO ₂	25.4 (10.1)	23.3 (8.0)	22.2 (7.1)	17.7(102)	22.2
	SO ₂	14.8 (4.9)	14.4 (3.9)	14.1(3.3)	14.4 (5.3)	14.4
	H ₂ O	854 (274)	364 (276)	747 (289)	474 (389)	610
^s Molar composition, %	H ₂ O	98.3	96.4	98.3	97.7	97.9

	CO ₂	1.20	2.53	1.18	1.49	1.44
	SO ₂	0.48	1.10	0.52	0.82	0.66
[^] Molar ratios	CO ₂ / SO ₂	2.48	2.33	2.31	1.80	2.22
	H ₂ O/ SO ₂	205	89.3	189	118	148
	H ₂ O/CO ₂	82.6	38.3	81.9	65.6	61.1

364



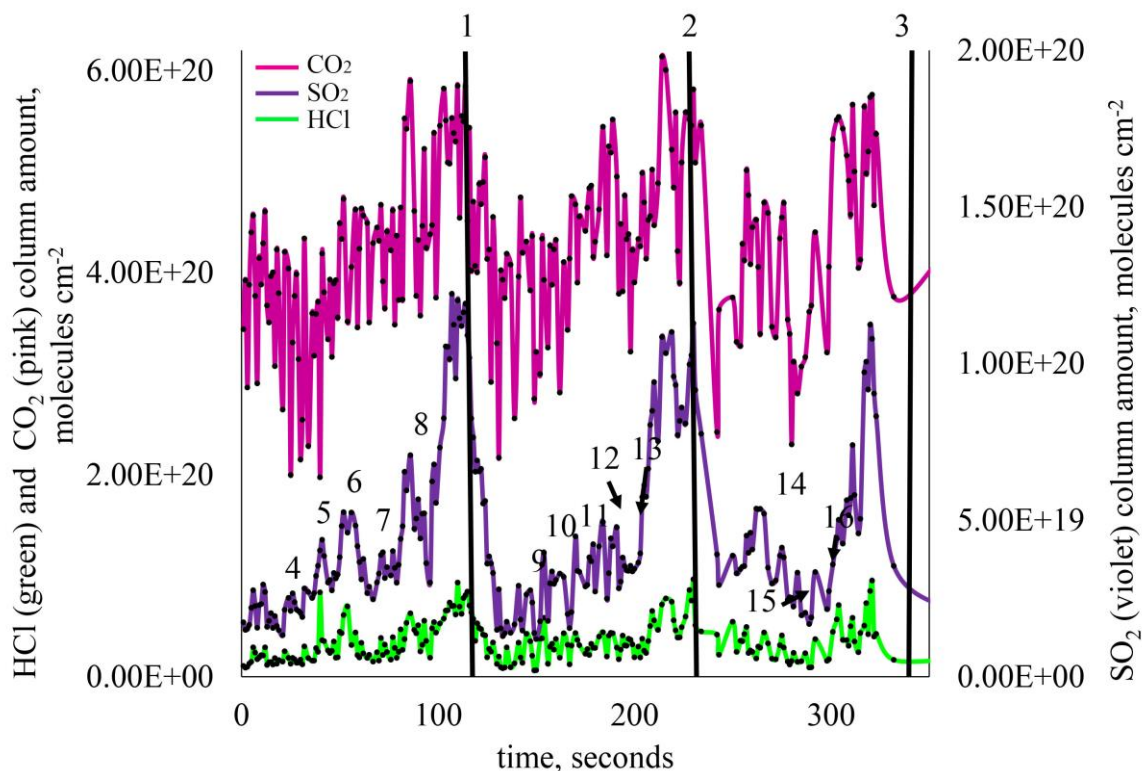
365

366 **Figure 4** H₂O/SO₂ ratio for a Multi-GAS measurement period on 16th July from 5:22 to 6:45 pm.
 367 Photos from (a) to (d) show the prevailing different eruption styles in North and South crater: (a,
 368 d): spattering activity in the Southern crater, (b) spattering and a mild strombolian eruption in the
 369 South crater and (c) mild strombolian eruption in the South crater and powerful strombolian
 370 eruption in the North crater. Both, the H₂O and the SO₂ content of the volcanic gases increases
 371 from spattering over mild to powerful strombolian eruptions. Eruptive events occur on average
 372 every 62 (sd: 30) seconds.

373 4.3 Volcanic gas composition from OP-FTIR spectroscopy

374 **Figure 5** shows the retrieved column amounts for HCl, CO₂, and SO₂ from the time series of
 375 set 1 from the South crater, which was obtained from the southern crater rim. The record
 376 identifies 16 explosions in 360 s (identified by the rapid increase in gas column amounts) and
 377 provides information about changes in gas ratios before and during explosions. We

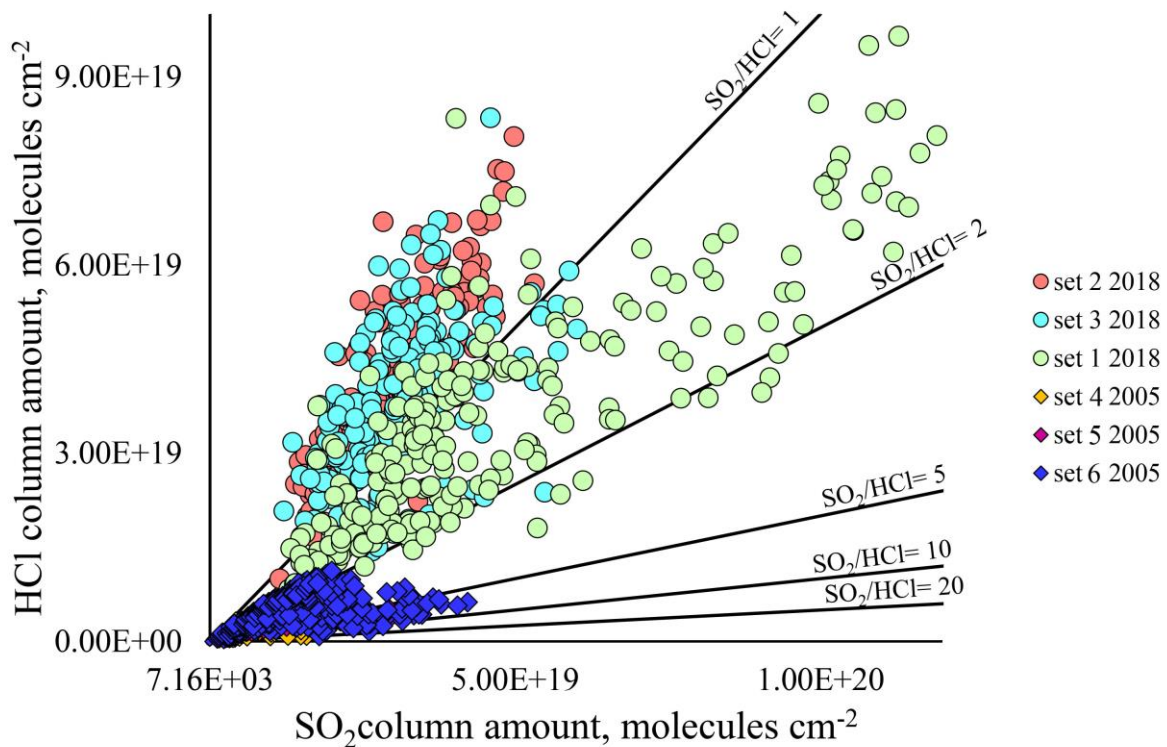
378 differentiate between active degassing, consisting of intermittent strombolian explosions and
379 spattering; and passive degassing.



380
381 **Figure 5** Time-series of retrieved column amounts of HCl (green), SO₂ (violet), CO₂ (red) for
382 data set 1, in molecules·cm⁻². Prominent strombolian explosions are numbered with 1, 2, 3 and
383 occur ~every 100 seconds. Numbered peaks from 4 to 16 mark minor explosive events prior to
384 the strombolian events.

385
386 A cyclicity is visible when less active periods are interrupted by explosions, identified by an
387 increase in SO₂ and CO₂ followed by a decrease (**figure 5**); explosions occur at the peaks of
388 these cycles. In set 1, explosions 1, 2 and 3 were accompanied by a rise in SO₂ column
389 amounts, followed by a decrease to pre-explosion column amounts of SO₂ after ~60 seconds.
390 Smaller explosions (4, 5, 7, 9, 10, 11, 13, and 16; **figure 5**) are associated with peaks in SO₂
391 column amounts up to $<4.93 \cdot 10^{19}$ molecules·cm⁻² after which SO₂ column amounts remain
392 elevated above the pre-explosion level. Explosions 6 and 8 were associated with increases in
393 SO₂ column amounts up to $5.26 \cdot 10^{19}$ and $7.07 \cdot 10^{19}$ molecules·cm⁻² respectively, which then
394 decreased after the explosions, returning to pre-explosion values after ~20 seconds. Variation
395 in the concentration-pathlengths of the measured gases could be also caused by the dilution
396 effect of wind gusts in the crater but we regard it unlikely as these changes occur
397 periodically, which is more consistent with the observed volcanic activity.

398
399



401

402 **Figure 6** Column amounts for SO_2 and HCl for spectra from set 1 (green circles; 06:41-06:56 h),
 403 set 2 (red circles; 08:19-08:24 h) set 3 (blue circles; 08:56-09:03 h) measured all from the same
 404 position on the South crater on 16 July 2018 and data from the South crater on 1 January 2005
 405 including set 4 (yellow diamonds: 09:19-09:22 h), set 5 (pink diamonds: 09:23-09:24 h) and set 6
 406 (blue diamonds: 09:24-09:25 h) (Oppenheimer et al., 2006). Solid lines indicate the SO_2/HCl
 407 ratios. Passive degassing is characterised by $\text{HCl} > \text{SO}_2$ whereas active degassing has higher SO_2
 408 concentrations ($\text{SO}_2 > \text{HCl}$). Higher ratios indicate a higher proportion of explosive gas. Set 1 is
 409 compared to set 2 and set 3 a period of higher activity. (Average HCl error: $\pm 7\%$ and SO_2 error:
 410 $\pm 4.8\%$).

411

412 We observe that active degassing from the South crater is distinguished by a molar SO_2/HCl
 413 ratio between 1 and 1.7 (**table 3**); whereas a $\text{SO}_2/\text{HCl} < 1$, where HCl is dominant compared
 414 to SO_2 in the gas phase, characterises the passive degassing periods (**table 3**). In 2005,
 415 Strombolian eruptions in the South crater emitted gas with molar $\text{SO}_2/\text{HCl} > 30$, and passive
 416 degassing was characterised by molar SO_2/HCl between 1.5 and 2.5 (Oppenheimer et al.,
 417 2006). Photos taken in 2005 revealed more violent eruptions occupying the whole crater and
 418 with a higher number of volcanic pyroclasts, ejected to greater heights (Oppenheimer et al.,
 419 2006). This violent type of eruption was not observed in July 2018. The composition of
 420 volcanic gases during active and passive phases is shown in **table 3**.

421

422 *Table 3: Mean chemical composition (as molar ratios) of volcanic gases emitted from Yasur Volcano,*
 423 *Vanuatu, during ‘active’ and ‘passive’ (non-explosive) phases on 16 July 2019. *South crater*
 424 *measured by OP-FTIR ; +Plume of North and South crater measured by MultiGAS. Uncertainties on*

425 the mean molar ratios are shown as a \pm range. Number of measurements in each case are shown in
 426 brackets.

427

<i>Molar ratio</i>	<i>Active phase</i>	<i>Passive phase</i>
⁺ H ₂ O/SO ₂	315 \pm 78.8 (222)	174 \pm 43.5 (477)
⁺ CO ₂ /SO ₂	2.85 \pm 0.17 (222)	1.96 \pm 0.12 (477)
[*] SO ₂ /HCl	1.7 \pm 0.22 (84)	0.5 \pm 0.07 (423)

428

429 4.4 Volcanic gas fluxes

430 In **table 4** we show the flux of SO₂, CO₂ and HCl from Yasur Volcano in 2018, derived from
 431 UV camera data and from the Multi-GAS and FTIR molar ratios (**table 2**) compared to those
 432 of other basaltic open vent volcanoes known for their strombolian activity. The mean SO₂
 433 flux has been measured as 7.9 kg·s⁻¹ (Bani and Lardi, 2007), 7.9 kg·s⁻¹ (Metrich et al., 2011)
 434 and 4.2 kg s⁻¹ in this study.

435 Combining the flux measured in 2018 with the mean mass ratios in the gas plume (**table 2**
 436 and the average SO₂/HCl value of 1.02) we calculate daily fluxes of 5.90 kg·s⁻¹ CO₂ (\pm 16.2
 437 %), 224 kg·s⁻¹ H₂O (\pm 29.2%) and 2.33 kg·s⁻¹ HCl (\pm 13.6%). In 2007 the corresponding
 438 fluxes were 9.7 kg·s⁻¹ CO₂ (64 % higher than in 2018), the HCl flux was 1.9 kg·s⁻¹ (18 %
 439 lower than in 2018) and the SO₂ flux was 7.9 kg·s⁻¹ (88 % higher than in 2018). We compare
 440 the active and passive CO₂/SO₂ and SO₂/HCl ratios with the overall mean ratios in order to
 441 get an estimate of the amount of gas supplied by active rather than passive degassing. For
 442 example, the mean molar CO₂/SO₂ is 2.14 and the gases emitted during active degassing
 443 periods have a CO₂/SO₂ of 2.85 and the passive degassing periods 1.96. Active degassing
 444 therefore provides 20% of the total gas flux. The same value (20%) is derived using the
 445 overall mean molar CO₂/SO₂ of 2.14 and the active and passive degassing ratios (2.85 and
 446 1.96). An SO₂ flux of 4.2 \pm 0.6 kg·s⁻¹ is the same as 363 \pm 54 tonnes of SO₂ per day, of which
 447 only ~ 73 tonnes per day is derived from active degassing, the rest passive degassing. Using a
 448 bubble burst frequency of every 0.02 seconds; we infer a bubble volume of 5095 m³.

449

450 *Table 4: Average volcanic gas composition (molar ratios) and fluxes (in kg·s⁻¹) emitted from Yasur*
 451 *Volcano, Vanuatu, in July 2018 Stromboli (Italy), Villarrica (Chile) and Masaya (Nicaragua).*

	<i>Yasur,</i> <i>Vanuatu</i>	<i>Stromboli,</i> <i>Italy</i>	<i>Villarrica,</i> <i>Chile</i>	<i>Masaya,</i> <i>Nicaragua</i>

Molar ratios	CO ₂ /SO ₂	2.14 ± 0.13 ^a	5.7 ^b ± 0.34 - 8 ^g ± 0.48	1.5 ^d ± 0.09 1.7 ^d ± 0.11	2.7 ± 0.3 ^e
	H ₂ O/SO ₂	190 ± 48 ^a	26.7 ^b ± 6.7 - 48.8 ^g ± 5.7	67 ^d ± 16.8- 75 ^d ± 18.8	63 ± 7 ^e
	SO ₂ /HCl	1.0 ± 0.14 ^a	1.00 ^h ± 0.08 -	3 ± 0.1 ^j 1.50 ^h ± 0.12	2 ± 0.03 ^e
Mass fluxes	SO ₂	4.2 ± 0.6 ^a	0.7 ^c ± 0.12 - 3.0 ± 0.45 ^g	1.5 ^d ± 0.18- 3.7 ⁱ ± 0.56	7.9 ± 2.37 ^e
	HCl	2.3 ± 0.34	0.4 ^{c,g} -1.1 ^{f,h}	0.3 ^{d,i} -0.7 ⁱ	2.2 ^e
	CO ₂	5.9 ± 0.94	2.6 ^{b,c} -15.8 ^{g,f}	1.5 ^d -4.1 ^{d,h}	13.9 ^e
	H ₂ O	224	5.2 ^{b,c} -41.2 ^{g,f}	28.3 ^d - 78.0 ^{d,h}	140 ^e
	Total gas	236	8.9-61.1	31.6-86.5	164

452

453 ^a This study: average composition 2018; ^b Aiuppa et al., 2010, ^c Tamburello et al., 2012, ^d Liu et al., 2018, ^e Martin et al.,
454 2010. ^fAllard ,2010, ^g Burton et al., 2007, ^h Sawyer et al., 2011,

455 5. Discussion

456 4.2 Gas evolution and outgassing in a crystal-rich conduit

457

458 We use geochemical data from Yasur's primitive melt inclusions in olivines (Metrich et al.,
459 2011) to generate a model of closed system magma degassing and compare it with the
460 measured gas composition at the surface (**table 3**) to infer the approximate pressure of last
461 gas-melt equilibration, which may be equivalent to the gas segregation pressure, for active
462 and passive modes of degassing. Extensive petrological study of Yasur magmas has led to a
463 model (**figure 7; table 5**) whereby primitive basaltic magmas enter the system at depths of >
464 6 km containing ~2500 ppm CO₂ (reconstructed from melt inclusion data and volcanic gas
465 ratios; Metrich et al., 2011), ~ 1 wt% H₂O, 0.1 wt% S and ~550 ppm Cl. We use the S
466 contents of the melt inclusions and the mean CO₂/SO₂ of the gas plume in 2018 to estimate a
467 'primary' (pre-degassing) melt CO₂ content. Using an average sulfur content of melt
468 inclusions of 0.1 wt. % (Metrich et al., 2011) and the average CO₂/SO₂ plume mass ratio of
469 1.5 in July 2018, we obtain a pre-degassing bulk melt CO₂ content of 3000 ppm, assuming
470 complete degassing of sulfur and CO₂ on eruption, compared with 2500 ppm estimated by
471 Metrich et al. (2011) using the same method.

472

473 At pressures between 330 and 130 MPa, the exsolved volatile phase is comprised almost
 474 entirely of CO₂ (resulting in the molar CO₂/SO₂ going to infinity at pressures >130 MPa in
 475 **figure 7**). The primitive basalt undergoes extensive crystallisation in a magma reservoir
 476 between 130 and 50 MPa (melt fraction remaining ~ 0.46) to produce basaltic-trachyandesite
 477 (Metrich et al., 2011). Olivine-hosted melt inclusions of basaltic-trachyandesite that are
 478 assumed to have originated in this reservoir contain up to 1 wt.% H₂O, 780 ppm S, 1200 ppm
 479 Cl and ~500 ppm CO₂ (Metrich et al., 2011). By this stage 63% of S, and 43% of bulk
 480 magmatic water content has been lost to the vapour phase. The exsolved volatile phase
 481 existing in equilibrium with the basaltic trachyandesite melt at this pressure has a molar
 482 CO₂/SO₂ of ~2.6, and molar SO₂/HCl >100 (**figure 7; table 5**).

483

484 Between 50 MPa (~ 2 km) and the surface ('stage II' of Metrich et al., 2011), S and Cl degas
 485 from the melt (**table 5; figure 7**). At the end of this stage, 29% of the Cl, 86% of the bulk S,
 486 and 90% of the bulk water has been lost from the magma (Metrich et al., 2011). The exsolved
 487 volatile phase is expected to have a molar CO₂/SO₂ of ~1.8-2.0 in this pressure interval, and a
 488 molar SO₂/HCl of 2-6 (**figure 7; table 5**). On eruption (stage III), an additional ~ 40% of Cl
 489 exsolved into a vapour phase, as well as an additional 8% S and 4% H₂O. This low pressure
 490 gas is highly enriched in HCl, generating a molar SO₂/HCl of < 3, with a molar CO₂/SO₂ of
 491 1.7 to 2 (**table 5; figure 7**).

492

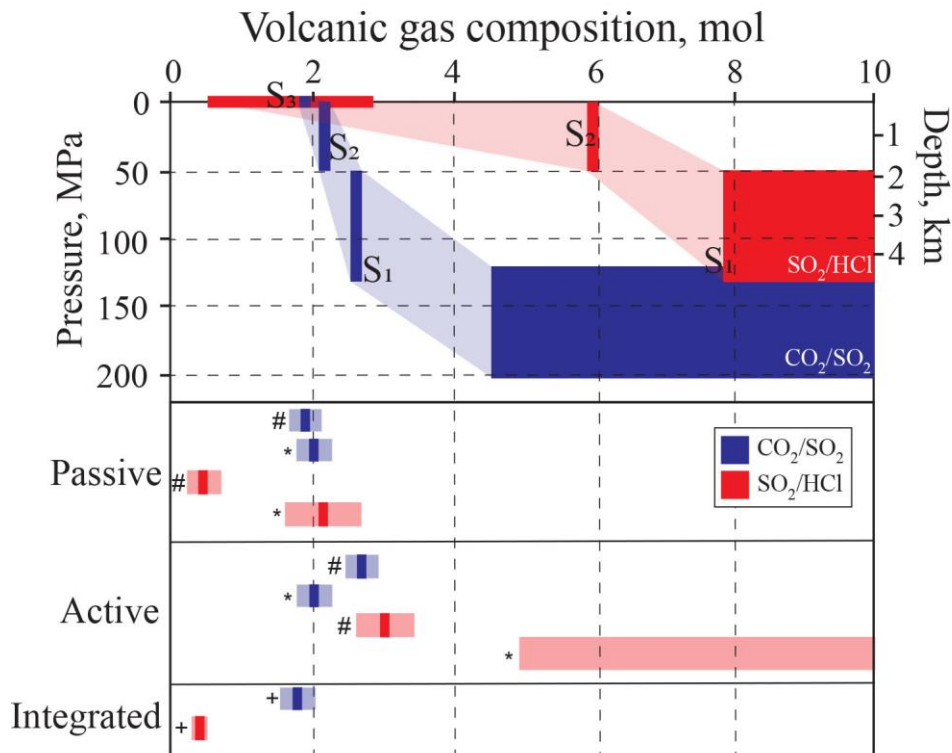
493 *Table 5 Yasur's melt composition from primitive melt inclusions (Metrich et al., 2011) and the*
 494 *calculated emitted amount and gas composition for degassing stage I,II, and III in a closed degassing*
 495 *system. The melt fraction in each stage was used to calculate the crystal fraction at each stage (1-f)*
 496 *and incorporate fractional crystallization in the melt degassing process.*

Stage	Pressure, MPa		Melt, wt%					f, melt fraction	Amount degassed, ppm				Volcanic gas ratios, molar	
	Max	Min	CO ₂	H ₂ O	S	Cl	Comp		K ₂ O ₀ /K ₂ O	ΔCO ₂	ΔH ₂ O	ΔS	ΔCl	CO ₂ /SO ₂
I	330	180	0.25	0.8	0.099	0.055	bas	1	0	0	0	0	∞	∞
	130	50	0.05	1.2	0.078	0.1235	bas-trach- and	0.46	4934	5391	1370	10	2.6	152
II	50	0	0.005	1.2	0.033	0.091	bas-trach- and	0.43	5763	6605	1972	369	2.1	5.9
III	0	0	0.001	0.2	0.006	0.046	bas-trach- and	0.35	7132	2087	2768	1111	1.9	2.8

497

498 We compare our gas data (**table 3**) as well as previously published data (Merich et al., 2011)
 499 to the model (**figure 7**). The gas compositions for passive degassing are consistent with gases
 500 being derived predominantly from the shallowest parts of the conduit system, at pressures of

501 <10 MPa (depths approximately <400 m). These gases are relatively enriched in HCl and
 502 have the lowest CO₂/SO₂ values. During the ‘active’ degassing (strombolian explosions and
 503 spattering), the gases become depleted in HCl and more CO₂-rich, consistent with their
 504 derivation from deeper in the conduit, perhaps down to 0.6 to 2 km depth (**figure 7**).



505
 506 **Figure 7** Predicted volcanic molar gas composition from melt inclusion data with pressure
 507 and depth for Yasur Volcano, reconstructed from melt inclusion data (Metrich et al., 2011).
 508 Molar CO₂/SO₂ is shown in blue, and molar SO₂/HCl in red. Depths are estimated using a
 509 crustal density of 2800 kg·m⁻³. Bottom: volcanic gas compositions measured at Yasur for
 510 passive degassing, active degassing (Strombolian activity) and measurements taken
 511 integrated over both passive and active periods. S₁-S₃ stands for different stages proposed in
 512 Metrich et al., 2011. Symbols denote data source. #: this study; *: Oppenheimer et al., 2006;
 513 +: Metrich et al., 2011. The dark rectangle denotes the mean value and the light shaded
 514 rectangle the range in probable values.

515
 516 Petrological studies have shown that between 6 and 1.8 km depth, the basaltic parent magma
 517 crystallises by > 46 vol% (Metrich et al., 2011) to produce the basaltic trachyandesites that
 518 are erupted. Erupted magmas contain around 30 vol% crystals (predominantly plagioclase
 519 phenocrysts up to 5 mm in size, and minor olivine, clinopyroxene and Fe-oxides; Metrich et
 520 al., 2011), which suggests that significant volumes of crystals (dominantly olivine) must
 521 accumulate in a subsurface mush pile. Extensive crystallisation in the upper 1-2 km of the
 522 conduit, driven by water degassing, induces changes in the rheological properties of the
 523 magma. We use the Giordano et al. (2008) viscosity model with a typical melt inclusion

524 composition from Metrich et al. (2011) and a H₂O content of 1.1 wt% for pre-degassing and
525 0.2 wt% after degassing. Based on the MELTS output the crystallinity increases from 10 to
526 32 vol% on degassing. We find that the bulk magma effective viscosity increases from 5.8 x
527 10² Pa·s prior to degassing to 1.5 x 10⁵ Pa·s after degassing and crystallisation.

528

529 In line with recent studies showing how the exsolved gas phase interacts with the crystal
530 phase (Belien et al., 2010, Parmigiani et al., 2014, 2016, 2018, Oppenheimer et al.,
531 2015,2020, Pistone et al., 2017, Barth et al., 2019, Spina et al., 2019b,), we suggest that the
532 increase in the crystallinity and bulk viscosity of the magma creates a plug at the top of the
533 conduit that develops an effective yield strength (figure 8). Our hypothesis is consistent with
534 previous work: Kremers et al., (2012) suggested that a degassed, viscous plug may exist in
535 the upper conduit of Yasur, based on the observed mingling of sideromelane and microlite-
536 rich tachylite. We envisage Yasur's shallow conduit consisting of a crystal-rich region with a
537 thickness of at least 0.6 and up to 2 km, if extensive crystallization is driven by H₂O
538 degassing (Metrich et al., 2011). Magmatic gas bubbles (with a slight CO₂-enrichment over
539 gases closer to the surface, and poor in HCl) will accumulate in the crystal-rich plug , before
540 generating a local overpressure that is sufficient to overcome the yield strength of the
541 overlying crystal plug (**figure 8a**). The gas bubble will then migrate upward (**figure 8b, c**)
542 and transport magma in its wake (Del Bello et al., 2015). At the surface, the bubble bursts as
543 a typical Strombolian eruption with a gas phase enriched in CO₂ compared to SO₂ (**figure**
544 **8d**). The plug rebuilds and bubbles begin to get trapped again and a new cycle starts (**figure**
545 **8g**). Bubbles released during 'passive degassing are sourced from close to the surface and in
546 general, these shallow gases are richer in HCl than the deeper accumulated gases due to the
547 fact that HCl exsolves at pressures < 10 MPa.

548

549 *4.3 Degassing rates and magma fluxes*

550 We may calculate the net upward flux of magma in the conduit required to supply the
551 observed fluxes of SO₂ at the surface (**table 4**). Using the maximum pre-eruptive sulphur
552 concentrations of 1000 ppm in primitive olivine-hosted melt inclusions (Metrich et al., 2011)
553 and mean SO₂ fluxes (9.9 to 1.2 kg·s⁻¹ with a mean of 4.1 kg·s⁻¹) measured on 8 July ,we infer
554 a magma supply rate between 770 and 6600 kg·s⁻¹, for a magma mean density of 2650 kg·m⁻³
555 and a crystallinity of 32 vol%. Our calculated bulk magma degassing rate of 2700 kg·s⁻¹ is
556 lower than previous estimates of magma degassing rate of 4100 kg·s⁻¹ (Metrich et al, 2011).

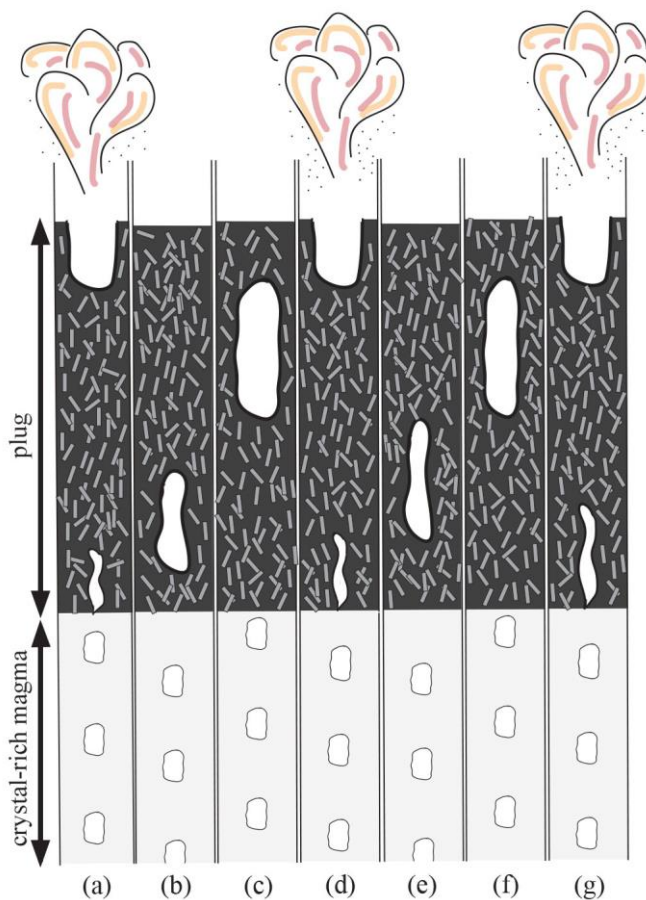
557 We assume in this calculation that the magma degasses all of its sulfur (the S concentration in
558 the erupted glass matrix is 0.006 wt.%). Yasur volcano has been degassing for the last 1400
559 years (Vergnolle and Metrich, 2016). Over long timescales the flux of degassing (but not
560 necessarily erupted) magma is 0.01 to 0.08 km³ per year, with a minimum of 13-109 km³
561 degassed magma presumably stored as a plutonic body at depth over 1400 years, consistent
562 with previous estimates (0.05 km³ per year; Metrich et al., 2011).

563

564 These new data from Yasur volcano in 2018 provide insights into the influence of crystals on
565 bubble formation events in the shallow conduit. These crystals may form a viscous plug that
566 influences bubble formation depth and consequently their chemical fingerprint. It is known
567 that magma in the shallow conduit of other Strombolian active volcanoes is crystal-rich, with
568 30 to 60 vol. %. This crystal content might be high enough to develop an effective yield
569 strength to trap bubbles and form slugs.

570

571



572

573 **Figure 8** Schematic diagram shows the shallow plumbing system of Yasur Volcano (from
574 600 bar to the surface). (Described in main text).

575 **Conclusions**

576 We present volcanic gas flux and composition data from Yasur Volcano, Vanuatu, during a
577 field campaign in July 2018. We draw the following conclusions:

578

579 (1) The average volcanic plume chemistry is characterised by a mean molar CO_2/SO_2
580 ratio of 2.14, $\text{H}_2\text{O}/\text{SO}_2$ of 190 and SO_2/HCl of 1.02. The mean SO_2 flux is $4.2 \text{ kg}\cdot\text{s}^{-1}$.
581 Therefore, the mean fluxes of the other species are $5.9 \text{ kg}\cdot\text{s}^{-1} \text{ CO}_2$, $224 \text{ kg}\cdot\text{s}^{-1} \text{ H}_2\text{O}$ and
582 $2.3 \text{ kg}\cdot\text{s}^{-1} \text{ HCl}$.

583

584 (2) The degassing regime at Yasur Volcano, as also defined from previous studies
585 (Oppenheimer et al., 2007; Metrich et al., 2011) ranges from ‘passive’ to ‘active’
586 styles, with the latter characterised by strombolian explosions. These styles are also
587 distinguished by their characteristic gas compositions in July 2018: (a) gases emitted
588 during active degassing are enriched in SO_2 and CO_2 with CO_2/S ratios of $2.85 \pm$
589 0.17 , SO_2/HCl with 1.7 ± 0.22 and $\text{H}_2\text{O}/\text{SO}_2$ with 315 ± 78.8 (b) passive degassing is
590 enriched in HCl with CO_2/SO_2 ratios of 1.96 ± 0.12 , SO_2/HCl with 0.50 ± 0.07 and
591 $\text{H}_2\text{O}/\text{SO}_2$ of 174 ± 43.5 .

592

593 (3) In order to understand the physical and chemical characteristics of the passive and
594 active degassing at Yasur, we consider the gas compositions in the context of a
595 volatile degassing model derived from melt inclusion studies (Metrich et al., 2011).
596 We envisage Yasur’s shallow conduit consisting of a crystal-rich region with a
597 thickness of at least 0.6 km, and up to 2 km from the surface. Magmatic gas bubbles
598 (with a slight CO_2 -enrichment over gases closer to the surface, and poor in HCl)
599 accumulate at the base of the crystal-rich plug, before generating a local overpressure
600 that is sufficient to overcome the yield strength of the overlying crystal plug.

601

602 **Acknowledgements**

603 We thank the Vanuatu Meteorology and Geohazards department for their collaboration and
604 support for during access and permission performing a field campaign at Yasur Volcano.
605 Furthermore, we gratefully acknowledge the loan of equipment to carry out this research
606 from the Natural Environment Research Council Field Spectroscopy Facility and their help in
607 during the fieldwork when any questions arose. We also thank Kelson and Rodga from
608 Jungle Oasis for their help during our stay on Tanna island. This work was supported by the
609 Natural Environment Research Council (grant number NE/L002507/1), by the postgraduate

610 travel funds received from Fitzwilliam College, by the Elspeth Matthews grant given by the
611 Royal Geological Society, by the Mary Euphrasia Mosley, Sir Bartle Frere and Worts travel
612 fund report given by the University of Cambridge and by the Exzellenzstipendium received
613 by WKO. A.A. acknowledges funding support from the Alfred P. Sloan Foundation via the
614 Deep Carbon Observatory (UniPa-CiW subcontract 10881-1262) and from MIUR (under
615 grant n. PRIN2017-2017LMNLAW). T.D.P. acknowledges the support of the Royal Society
616 (RG170226). TI is a Commonwealth Rutherford Fellow, funded by the UK government. We
617 thank two anonymous reviewers, whose helpful comments improved the manuscript
618 enormously.

619

620

621 **References**

622 Aiuppa, A., Guidice, G., Gurrieri, S., Liuzzo, M., Burton, M., Caltabiano, T., McGonigle,
623 A.J.S., Salerno, G., Shinohara, H., Valenza, M., 2008. Total volatile flux from Mount Etna. *J.*
624 *Geophys. Res. Lett.* 35, L24302

625

626 Aiuppa, A., Bertagnini, A., Metrich, N., Moretti, R., Di Muro, A., Liuzzo, M., Tamburello,
627 G., 2010. A model of degassing for Stromboli volcano. *Earth Planet. Sci. Lett.* 294, 195-204.

628

629 Aiuppa, A., de Moor, J. M., Arellano, S., Coppola, D., Francofonte, V., Galle, B.,
630 Moretti, R., 2018. Tracking formation of a lava lake from ground and space: Masaya volcano
631 (Nicaragua), 2014–2017. *Geochem. Geophys. Geosyst.* 19, 496–515.

632

633 Aiuppa, A., Fischer, T.P., Plank, T., Bani, P., 2019. CO₂ flux emissions from the Earth's
634 most actively degassing volcanoes, 2005-2015. *Sci. Rep.* 9(5442).

635

636 Allard, P., Carbonelle, J., Metrich, N., Loyer, H., Zettwoog, P., 1994. Sulphur output and
637 magma degassing budget of Stromboli volcano. *Nature* 368, 326-330.

638

639 Allard, P., Burton, M.R., Mure, F., 2005. Spectroscopic evidence for a lava fountain driven
640 by previously accumulated magmatic gas, *Nature* 433, 407–410.

641

642 Allard, P., A CO₂-rich gas trigger of explosive paroxysms at Stromboli basaltic volcano,
643 Italy. 2010. *J. Volcanol. Geotherm. Res.* 189, 363-374.

644

646 Andres, R.J., Kasgnoc, A.D., 1998. A time-averaged inventory of subaerial volcanic sulfur
647 emissions. , *J. Geophys. Res.* 103, 25251-25261.

648

649 Bani, P., Lardy, M., 2007. Sulphur dioxide emission rates from Yasur volcano, Vanuatu
650 archipelago. *Geophys. Res. Lett.* 34.

651

652 Bani, P., Harris, A. J.L., Shinohara, H., Donnadieu, F., 2013. Magma dynamics feeding
653 Yasur's explosive activity observed using thermal infrared remote sensing. *Geophys. Res.*
654 *Lett.* 40, 3830-3835.

655
656
657 Barth, A., Edmonds, E., Woods, A.W., 2019. Valve-like dynamics of gas flow through a
658 packed crystal mush and cyclic strombolian explosions. *Sci Rep.* 9(1), 821.
659
660 Batchelor, G.K., 1967. *An Introduction to Fluid Dynamics.* Cambridge University Press, 615
661 pp
662
663 Battaglia, J., Métaixian, J.P., Garaebiti, E., 2016. Families of similar events and modes of
664 oscillation of the conduit at Yasur volcano (Vanuatu). *J. Volcanol. Geotherm. Res.* 322, 196-
665 211.
666
667 Battaglia, J., Métaixian, J.P., Garaebiti, E., 2016. Short term precursors of Strombolian
668 explosions at Yasur volcano (Vanuatu), *Geophys. Res. Lett.* 43
669
670 Blackburn E.A., Wilson, L., Sparks, R.S.J., 1976. Mechanism and dynamics of Strombolian
671 activity. *J. Geol. Soc. Lond.* 132, 429-440.
672
673 Beckett, F.M., Burton, M., Mader, H.M., Phillips, J.C., Polacci, M., Rust, A.C., Witham, F.,
674 2014. Conduit convection driving persistent degassing at basaltic volcanoes. *J. Volcanol.*
675 *Geotherm. Res.* 238, 19-35.
676
677 Belien, I.B., Cashmann, K.V., Rempel, A.W., 2010. Gas accumulation in particle-rich
678 suspensions and implications in crystal-rich magma. *Earth Planet. Sci. Lett.* 297, 133-140.
679
680 Bell, R.J., 1972. *Introductory Fourier transform spectroscopy.* Academic Press, Inc., New
681 York.
682
683 Burton, M. R., Oppenheimer, C., Horrocks, L.A., Francis, P.W., 2000. Remote sensing of
684 CO₂ and H₂O emission rates from Masaya volcano, Nicaragua. *Geology* 28, 915 – 918.
685
686 Burton, M., Allard, P., Mure, F., La Spina, A., 2007a. Magmatic gas composition reveals the
687 source depth of slug-driven Strombolian explosive activity. *Science* 317, 227-230.
688
689 Burton, M.R., Mader, H.M., Polacci, M., 2007b. The role of gas percolation on quiescent
690 degassing of persistently active basaltic volcanoes *Earth Planet. Sci. Lett.* 262, 46-60.
691
692 Burton, M.R., Sawyer, G.M., Granieri, D., 2013. Deep Carbon Emissions from Volcanoes.
693 *Rev. Mineral. Geochem.* 75, 323-354.
694
695 Capponi, A., James, M.R., Lane, S.J., 2016. Gas slug ascent in a stratified magma:
696 Implications of flow organisation and instability for Strombolian eruption dynamics. *Earth*
697 *Planet. Sci.* 435, 159-170.
698
699
700 Carn, S.A., Fioletov, V.E., McLinden, C.A., Li, C., Krotov, N.A., 2017. A decade of global
701 volcanic SO₂ emissions measured from space. *Sci Rep.* 7.
702

703 Carney, J., Macfarlane, A., 1979. Geology of Tanna, Aneityum Futana and Aniwa. New
704 Hebrides Gov. Geol. Surv.Rep. 5-29.
705

706 Chouet, B., Saccorotti, G., Dawson, P., Martini, M., Scarpa, R., DeLuca, G., Milana, G.,
707 Cattaneo, M., 1999. Broadband measurements of the sources of explosions at Stromboli
708 volcano, Italy. *Geophys. Res. Lett.* 26, 1937–1940.

709 Chouet, B., Dawson, P., Ohminato, T., Martini, M., Saccorotti, G., Giudicepietro, F., De
710 Luca, G., Milana, G., Scarpa, R., 2003. Source mechanisms of explosions at Stromboli
711 Volcano, Italy, determined from moment-tensor inversions of very-long-period data. *J.*
712 *Geophys. Res.* 108.

713 Cimarelli, C., Costa, A., Mueller, S., Mader, H.M., 2011. Rheology of magmas with bimodal
714 crystal size and shape distributions: Insights from analogue experiments. *Geochem. Geophys.*
715 *Geosyst.* 12, 1525-2027.
716

717 Coltelli, M., Del Carlo, P., Vezzoli, L., 1995, Stratigraphy of the Holocene Mt. Etna
718 explosive eruptions: *Periodico di Mineralogia*, 64, 141–143.
719

720 Del Bello, E., Llewellyn, E., Taddeucci, J., Scarlato, P., Lane, J. S., 2012. An analytical
721 model for gas overpressure in slug-driven explosions: Insights into Strombolian volcanic
722 eruptions. *J. Geophys. Res.* 117.
723

724 Duffell, H.J., Oppenheimer, C., Pyle, D.M., Galle, B., McGonigle, A.J.S., Burton, M.R.,
725 2003. Changes in gas composition prior to minor explosive eruption at Masaya volcano,
726 Nicaragua. *J. Volcanol. Geotherm. Res.* 126, 327-339.
727

728 Del Gaudio, P., Ventura, G., Taddeucci, J., 2013. The effect of particle size on the rheology
729 of liquid-solid mixtures with the application to lava flows: Results from analogue
730 experiments. *Geochem. Geophys. Geosyst.* 14, 2661-2669.
731

732 Francis, P. W., Oppenheimer, C., Stevenson, D., 1993. Endogenous growth of persistently
733 active volcanoes. *Nature* 366, 554–557.
734

735 Francis, P., and Oppenheimer, C., 2004. *Volcanoes*, 2nd Edition, Oxford University Press,
736 Oxford, 521 pp.
737

738 Ghiorso, M.S., and Sack, R.O., 1995. Chemical mass transfer in magmatic processes IV. A
739 revised and internally consistent thermodynamic model for the interpolation and
740 extrapolation of liquid-solid equilibria in magmatic systems at elevated temperatures and
741 pressures. *Contributions Mineral. Petrol.* 1999, 197-212.
742

743 Girona, T., Costa, F., Schubert, G., 2015. Degassing during quiescence as a trigger of magma
744 ascent and volcanic eruptions. *Sci.Rep.* 5, 18212.
745

746 Gaudin, D., Taddeucci, J., Scarlato, P., Moroni, M., Freda, C., Gaeta, M., Palladino, D.M.,
747 2014. Pyroclastic tracking velocimetry illuminates bomb ejection and explosion dynamics at
748 Stromboli (Italy) and Yasur (Vanuatu) volcanoes. *J. Geophys. Res.* 119, 5384-5397.
749

750 Gaudin, D., Taddeucci, J., Houghton, B.F., Orr, T.R., Andronico, D., Del Bello, E., Kueppes,
751 U., Ricci, T., Scarlato, P., 2016. 3-D high speed imaging of volcanic bomb trajectory in
752 basaltic explosive eruptions. *Geochem. Geophys. Geosyst.* 17, 4268-4275.

753 Gaudin, D., Taddeucci, J., Scarlato, P., Del Bello, E., Ricci, T., Orr, T., Houghton, B., Harris,
754 A.J.L., Rao, S., Bucci, A., 2017. Integrating puffing and explosions in a general scheme for
755 Strombolian-style activity. *J. Geophys. Res. Solid Earth* 122 (3), 1860–1875.
756

757 Getson, J.M., Whittington, A.G., 2007. Liquid and magma viscosity of anorthite-forsterite-
758 diopside-quartz systems and implications for the viscosity-temperature paths of cooling
759 magmas. *J. Geophys. Res.* 112.

760

761 Griffiths, P.R., 1975. *Chemical infrared Fourier transform spectroscopy, Chemical analysis.*
762 Wiley, New York.
763

764 Gurioli, L., Colo, L., Bollasina, A.J., Harris, A.J.L., Whittington, A., Ripepe, M., 2014.
765 Dynamics of Strombolian explosions: Inferences from field and laboratory studies of erupted
766 bombs from Stromboli volcano, *J. Geophys. Res. Solid Earth*, 119, 319–345.
767

768 Harrocks, L. A., Oppenheimer, C., Burton, M.R., Duffell, H.J., Davies, N.M., Nicholas,
769 A.M., Bell, W., 2001. Open-path Fourier transform infrared spectroscopy of SO₂: An
770 empirical error budget analysis, with implications for volcano monitoring. *J. Geophys. Res.*
771 106, 27647-27659.
772

773 Harris, A.J.L., Stevenson, D.S., 1997. Magma budgets and a steady-state activity of Vulcano
774 and Stromboli. *Geophys. Res. Lett.* 24, 1043-1046.
775

776 Hort, M., Seyfried, R., Voge, M., 2003. Radar Doppler velocimetry of volcanic eruptions:
777 theoretical considerations and quantitative documentation of changes in eruptive
778 behaviour at Stromboli volcano, Italy. *Geophys. J. Int.* 154, 515–532.
779

780 Houghton, B.F., and Gonnermann, H.M., 2008. Basaltic explosive volcanism: Constraints
781 from
782 deposits and models. *Chem Erde-Geochem.* 68, 117-140.
783

784 Houghton, B.F., Taddeucci, J., Andronico, D., Gonnermann, H.M., Pistolesi, M., Patrick,
785 M.R., Orr, T.R., Swanson, D.A., Edmonds, M., Gaudin, D., Carey, R.J., Scarlato, P., 2016.
786 Stronger or longer: discriminating between Hawaiian and Strombolian eruption styles.
787 *Geology* 44, 163–166.

788 Huppert, H.E., Hallworth, M.A., 2007. Bi-directional flows in constrained systems. *J. Fluid*
789 *Mech.* 578, 95–112.

790 Ilanko, T., Oppenheimer, C., Burgisser, A., Kyle, P., 2015. Transient degassing events at the
791 lava lake at the lava lake of Erebus volcano. *GeoResJ*, 7, 43-48.
792

793 Ilyinskaya, E., Martin, R.S., Oppenheimer, C., 2012. Aerosol formations in basaltic lava
794 fountaining: Eyjafjallajökull volcano, Iceland. *J. Geophys. Res.* 117.
795

796 James, M.R., Lane, S.J., Wilson, L., Corder, S.B., 2009. Degassing at low magma-viscosity
797 volcanoes: Quantifying the transition between bubble-burst and Strombolian eruption. *J.*
798 *Volcanol. Geotherm. Res.*, 180, 81-88.
799

800 Jaupart, C., Vergnolle, S., 1989. The generation and collapse of a foam layer at the roof of a
801 basaltic magma chamber. *J. Fluid Mech.* 203, 347-380.
802

803 Jaupart, C., Vergnolle, S., 1988. Laboratory models of Hawaiian and Strombolian eruptions.
804 *Nature* 331, 58-60.
805

806 Kantzas, E.T., McGonigle, A.J.S., Tamburello, G., Aiuppa, A., Bryant, R.G., 2010. Protocols
807 for UV camera volcanic SO₂ measurements. *Volcanol. Geotherm. Res.* 194, 55-60.
808

809 Kazahaya, K., Shinohara, H., Saito, G., 1994. Excessive degassing of Izu-Oshima volcano:
810 magma convection in a conduit. *Bull. Volcanol.* 56, 207-216.
811

812 Kern, C., Luebcke, P., Bobrowski, N., Campion, R., Mori, T., Smekesn, J., Stebel, K.,
813 Tamburello, G., Burton, M., Platt, U., Prata, F., 2015. Intercomparison of SO₂ camera system
814 for imaging volcanic gas plumes. *Volcanol. Geotherm. Res.* 300, 22-36.

815 Kremers, S., Lavallée, Y., Hanson, J., Hess, K. U., Chevrel, M. O., Wassermann, J.,
816 Dingwell, D. B., 2012. Shallow magma - mingling - driven Strombolian eruptions at Mt.
817 Yasur volcano, Vanuatu *Geophys. Res. Lett.* 39(21).
818

819 Koyaguchi, T., 1985, Magma mixing in a conduit. *J. Volcanol. Geotherm. Res.* 25, 365-369.
820

821 Koyaguchi, T., 1987, Magma mixing in a squeezed conduit. *Earth Planet. Sci. Lett.* 84, 339-
822 744.
823

824

825 Liu, E.J., Wood, K., Mason, E., Edmonds, M., Aiuppa, A., Guidice, G., Bitetto, M.,
826 Francofonte, V., Burrow, S., Richardson, T., Watson, M., Pering, T.D., Wilkes, T.C.,
827 McGonigle, A.J.S., Velasquez, G., Melgarejo, C., Bucarey, C., 2019. Dynamics of
828 Outgassing and Plume Transport Revealed by Proximal Unmanned Aerial Systems (UAS)
829 Measurements at Volcan Villarrica, Chile. *Geochem. Geophys. Geosyst.*, 20,730–750.
830

831 Louat, R., Hamburger, M., Monizier, M., 1988. Shallow and intermediate-depth seismicity in
832 the New Hebrides arc: Constrains on the subduction process. In: Greene,H.G., Wong, F.L
833 (Eds), *Geology and Offshore Resources of Pacific Island Arcs- Vanuatu Region.* Circum-Pac.
834 Counc. For energy and Miner. Res., Houston, Tex., earth. Sci. Ser. 8, 329-356.
835

836 Martin. R.S., Sawyer, G.M., Spampinato, L., Salerno, G.G., Ramirez, C., Ilyinskaya, I., Witt,
837 M.L.I., Mather, T.A., Watson, I.M., Phillips, J.C., Oppenheimer, C., 2010. A volatile
838 inventory for Masya Volcano, Nicaragua. *Geophys. Res.* 115, B09215,
839

840 Meier, K., Hort, M., Wassermann, J., Garaebiti, E., 2016. Strombolian surface activity
841 regimes at Yasur volcano, Vanuatu, as observed by Doppler radar infrared camera and
842 infrasound. *J. Volcanol. Geotherm. Res.* 322, 184-195.
843

844 Metrich, N., Allard, P., Aiuppa, A., Bani, P., Bertagnini, A., Shinohara, H., Parello, F., Di
845 Muro, A., Garaebiti, E., Belhadj, O., Massare, D., 2011. Magma and volatile supply to post-
846 collapse volcanism and block resurgence in Siwi Caldera (Tanna island, Vanuatu Arc).
847 *J. Petrol.* 52, 1077-1105.

848
849 Mori, T., Burton, M., 2006. The SO₂ camera: A simple, fast and cheap method for ground
850 based imaging of SO₂ in volcanic plumes. *Geophys. Res. Lett.* 33.

851
852 Mori, T., Burton, M., 2009. Quantification of the gas mass emitted during single explosions
853 on Stromboli with the SO₂ camera. *J. Volcanol. Geotherm. Res.* 188, 395-400.

854
855 Neuberg, J., Lockett, R., Ripepe, M., Braun, T., 1994. Highlights from a seismic broadband
856 array on Stromboli volcano. *Geophys. Res. Lett.* 21, 749–752.

857
858 Ntepe, R., Dorel, J., 1990. Observation of seismic volcanic signals at Stromboli Volcano
859 (Italy). *J. Volcanol. Geotherm. Res.* 43, 235-251.

860
861 Oppenheimer, C., 1996. On the role of hydrothermal systems in the transfer of volcanic
862 sulfur to the atmosphere. *Geo-phys. Res. Lett.* 23, 2057-2060.

863
864 Oppenheimer, C., *Volcanic degassing*, In: *The Crust*, Vol. 3, *Treatise on Geochemistry*. 2003.
865 ed. by R.L. Rudnick, H.D. Holland, K.K. Turekian. Elsevier-Pergamon, Oxford, 123–166 .

866
867 Oppenheimer, C., Bani, P., Calkins, J.A., Burton, M.R., Sawyer, G.M., 2006. Rapid FTIR
868 sensing of volcanic gases released by Strombolian explosions at Yasur volcano. *Applied*
869 *Physics B*, Volume 85, Issue 2-3, 453-460.

870
871 Oppenheimer, J., Rust, A.C., Cashman, K.V., Sandnes, B., 2015. Gas migration regimes and
872 outgassing in particle-rich suspensions. *Front. Phys.* 3:60.

873
874 Oppenheimer, J., Capponi, A., Cashman, K.V., Lane, S.J., Rust, A.C., James, M.R., 2020.
875 Analogues experiments on the rise of large bubbles through a solids-rich suspension: A
876 “weak plug” model for Strombolian eruptions. *Earth Planet. Sci. Lett.* 531, 115931.

877
878 Patrick, M.R., Harris, A., Ripepe, M., Dehn, J., Rothery, D.A., Calvari, S., 2007. Strombolian
879 explosive styles and source conditions: Insights from thermal (FLIR) video. *Bull. Volcanol.*
69 (7), 769–784.

880
881 Parfitt, E.A., Wilson, L., 1995. Explosive volcanic eruptions: IX. The transition between
882 Hawaiian-style lava fountaining and Strombolian explosive activity. *Geophys. J. Int.*
121, 226–232.

883
884 Parfitt, E. A., 2004. A discussion of the mechanisms of explosive basaltic eruptions. *J.*
885 *Volcanol. Geotherm. Res.* 134, 77-107.

886
887 Parfitt, E.A., Wilson, L., 2008. *Fundamentals of physical volcanology*. Blackwell Publishing
888 Ltd. 230pp.

889 Parmigiani, A., Huber, C., Bachmann, O., 2014. Mush microphysics and the reactivation of
890 crystal-rich magma reservoirs. *J. Geophys. Res. Solid Earth* 119, 6308-6322.
891

892 Parmigiani, A., Faroughi S., Huber, C., Bachmann, O., Su, Y., 2016. Bubble accumulation
893 and its role in the evolution of the magma reservoirs in the upper crust. *Nature* 532, 492-495.
894

895 Parmigiani, A., Degruyter, W., Leclaire, S., Huber, C., Bachmann, O., 2017. The mechanics
896 of shallow magma reservoir outgassing. *Geochem. Geophys. Geosyst.* 18, 2887-2905.
897

898 Patrick, M.R., Harris, A.J.L., Ripepe, M., Dehn, J., Rothery, D., Calvari, S., 2007.
899 Strombolian explosive styles and source conditions: insights from thermal (FLIR) video.
900 *Bull. Volcanol.* 69, 769–784.

901 Pering, T.D., Tamburello, G., McGonigle, A.J.S., Aiuppa, A., James, M.R., Lane, S.J.,
902 Sciotto, M., Cannata, A., Patane, D., 2015. Dynamics of mild strombolian eruptions on Mt.
903 Etna. *J. Volcanol. Geotherm. Res.* 300, 103-111.
904

905 Pering, T.D., McGonigle, A.J.S., 2018. Combining Spherical-Cap and Taylor Bubble Fluid
906 Dynamics with Plume Measurements to Characterize Basaltic Degassing. *Geoscience* 8 (2),
907 42.
908

909 Pioli, L., Bonadonna, C., Azzopardi, B.J., Phillips, J.C., Ripepe, M., 2012. Experimental
910 constraints on the outgassing dynamics of basaltic magmas, *J. Geophys. Res.* 117, B03204,
911

912 Pistone, M., Whittington, A. G., Andrews, B. J., Cottrell, E. 2017. Crystal-rich lava dome
913 extrusion during vesiculation: an experimental study. *J. Volcanol. Geotherm. Res.* 347, 1–14.
914

915 Ripepe, M., Marchetti, E., 2002. Array tracking of infrasonic sources at Stromboli volcano.
916 *Geophys. Res. Lett.* 29.
917

918

919 Ripepe, M., Rossi, M., Saccorotti, G., 1993. Image processing of explosive activity at
920 Stromboli, *J. Volcanol. Geotherm. Res.* 54, 335–351.

921 Ripepe, M., Marchetti, E., Olivieri, G., 2007. Infrasonic monitoring at Stromboli volcano
922 during the 2003 effusive eruption: insights on the explosive and degassing process of an open
923 conduit system. *J. Geophys. Res.* 112, B09207.

924 Ripepe, M., Harris, A.J.L., 2008. Dynamics of the 5 April 2003 explosive paroxysm
925 observed at Stromboli by a near-vent thermal, seismic and infrasonic array. *Geophys. Res.*
926 *Lett.* 35
927 , L07306.
928

929 Rothman, L.S., Gordon, I.E., Barbe, A., Chris Benner, D., Bernath, P.F., Birk, M., Boudon,
930 V., Brown, L.R., Campargue, A., Champion, J.-P., Chance, K., Coudert, L.H., Dana, V.,
931 Devi, V.M., Fally, S., Flaud, J.-M., Gamache, R.R., Goldman, A., Jacquemart, D., Kleiner, I.,
932 Lacombe, N., Lafferty, W.J., Mandin, J.-Y., Massie, S.T., Mikhailenko, S.N., Miller, C.E.,
933 Moazzen-Ahmadi, N., Naumenko, O.V., Nikitin, A.V., Orphal, J., Perevalov, V.I., Perrin, A.,
934 Predoi-Cross, A., Rinsland, C.P., Rotger, M., Simeckova, M., Smith, M.A.H., Sung, K.,

- 935 Tashkun, S.A., Tennyson, J., Toth, R.A., Vandaele, A.C., Vander Auwera, 2009. The
936 HITRAN 2008 molecular spectroscopic database. *J. Quant. Spectrosc. Radiat. Transfer*
937 110:533–572.
- 938 Rosi, M., Pistolesi, M., Bertagnini, A., Landi, P., Pompilio, M., Di Roberto, A., 2013.
939 Stromboli Volcano, Aeolian Islands (Italy): Present Eruptive Activity and Hazards.
940 *Geological Society London Memoirs* 37(1), 473–490.
- 941
942 Sawyer, G.M., Salerno, G.G., Le Bond, J.S., Martin, R.S., Spampinato, L., Roberts, T.J.,
943 Mather, T.A., Witt, M.L.I., Tsanev, V.I., Oppenheimer, C., 2011. Gas and aerosol emissions
944 from Villarrica volcano, Chile. *J. Volcanol. Geotherm. Res.* 203, 62-75.
- 945 Shinohara, H., 2005. A new technique to estimate volcanic gas composition: plume
946 measurements with a portable multi-sensor system. *J. Volcanol. Geotherm. Res.* 143(4), 319–
947 333.
- 948 Slezin, Y.B., 2003. The mechanism of volcanic eruptions (a steady state approach). *J.*
949 *Volcanol. Geotherm. Res.* 122, 7–50.
- 950 Sparks, R.S.J., 1978. The dynamics of bubble formation and growth in magmas: A review
951 and analysis. *J. Volcanol. Geotherm. Res.* 3, 1-37.
- 952
953 Spina, L., Taddeucci, J., Cannata, A., Gresta, S., Lodato, L., Privitera, E., Scarlato, P., Gaeta,
954 M., Gaudin, D., Palladino, D.M., 2016. Explosive volcanic activity at Mt. Yasur: A
955 characterization of the acoustic events (9-12th July 2011). *J. Volcanol. Geotherm. Res.* 322,
956 174-183.
- 957 Spina, L., Morgavi, D., Costa, A., Scheu, B., Dingwell, D. B., & Perugini, D., 2019b. Gas
958 mobility in rheologically-layered volcanic conduits: The role of decompression rate and
959 crystal content on the ascent dynamics of magmas. *Earth Planet. Sci.* 524, 115732.
- 960 Stevenson, D.S., Blake, S., 1998. Modelling the dynamics and thermodynamics of volcanic
961 degassing. *Bull. Volcanol.* 60, 307–317.
- 962 Seyfried, R., Hort, M., 1999. Continuous monitoring of volcanic eruption dynamics: a review
963 of various techniques and new results from a frequency-modulated radar Dopplersystem.
964 *Bull. Volcanol.* 60, 627–639.
- 965 Symonds, R.B., Rose, W.I., Bluth, G.J.S., and Gerlach, T.M., 1994. Volcanic gas studies:
966 Methods, results, and applications, in Carroll, M.R., et al., eds., *Volatiles in magmas: Reviews*
967 *in Mineralogy*, v. 30, p. 1–66.
- 968
969 Taddeucci, J., Scarlato, P., Capponi, A., Del Bello, E., Cimarelli, C., Palladino, D.M.,
970 Keuppers, U., 2012a. High-speed imaging of Strombolian explosions: The ejection velocity
971 of pyroclasts. *Geophys.Res.Lett.* 39 (L02) 301.
- 972
973 Taddeucci, J., Alatoore-Ibarguengorita, M.A., Moroni, M., Tornetta, L., Capponi, A.,
974 Scarlato, P., Dingwell, D.B., De Rita, D., 2012 b. Physical parameterization of Strombolian
975 eruptions via experimentally-validated modeling of high-speed observations. *Geophys. Res.*
976 *Lett.* 39, L16306.

977
978 Tamburello, G., Aiuppa, A., Kantzas, E.P., McGonigle, A.J.S., Ripepe, M., 2012. Passive vs.
979 active degassing modes at an open-vent volcano (Stromboli, Italy). *Earth Planet. Sci. Lett.*
980 249-360, 106-116.
981
982 Tamburello, G., 2015. Ratiocalc: Software for processing data from multicomponent volcanic
983 gas analyzers. *Comput.Geosci.*82, 63-67.
984
985 Taylor, G.A., 1956. Review of volcanic activity in the Territory of Papua-New Guinea-the
986 Solomon and New-Hebrides Islands,1951-1953. *Bull.Volcanol.*, II/XVII, 33-37.

987 Urbanski, N., Voegelé, M., Seyfried, R., Ruepke, L., Petersen, T., Hanebuth, T., Hort, M., 2002.
988 15 days of continuous activity survey at Stromboli volcano/Italy in late September 2000:
989 Doppler radar, seismicity, infrared, soil humidity, and mapping of the crater region. *Int. J.*
990 *Earth Sci.* 91, 712–721.

991 Vergnolle, S., Brandeis, G., Marechal. 1996. Strombolian explosions 2: Eruption dynamics
992 determined from acoustic measurements. *J. Geophys. Res.* 101 (B9), 20449-20466.

993 Vergnolle, S., Ripepe, M., 2008, From Strombolian explosions to fire fountains at Etna
994 Volcano (Italy): What do we learn by acoustic measurement?, in *Fluid Motions in Volcanic*
995 *Conduits: A Source of Seismic and Acoustic Signals*, edited by S. J. Lane and J. S. Gilbert,
996 *Geol. Soc. Spec.Publ.* 307, 103–124.

997 Vergnolle, S., Metrich, N., 2016. A bird’s eye view of “Understanding volcanoes in the
998 Vanuatu arc”. *J. Volcanol. Geotherm. Res.* 322, 1-5.
999
1000
1001
1002 Walker, G. P. L., Self, S., and Wilson, L., 1984, Tarawera, 1886, New Zealand-A basaltic
1003 plinian fissure eruption. *J. Volcanol. Geotherm. Res.* 21, 61–78.
1004
1005 Williams, S. N., 1983, Plinian airfall deposits of basaltic composition: *Geology*, 11, 211–214.
1006
1007 Wilkes, C.T., Pering, T.D., McGonigle, A.J.S., Tamburello, G., Willmott, J.R., 2017. A Low-
1008 Cost Smartphone Sensor-Based UV Camera for Volcanic SO₂ Emission Measurements.
1009 *Remote Sens.* 2017, 9(1), 27.

1010 Wilson, L., Head, J.W., 1981. Ascent and eruption of basaltic mag-ma on the Earth and
1011 Moon. *J. Geophys. Res.* 86, 2971–3001.

1012 Wilson, L., Head, J.W., 1983. A comparison of volcanic eruption processes on Earth, Moon,
1013 Mars, Io and Venus. *Nature* 302,663–669.

1014 Woods, A.W., and Cardoso, S.S.S., 1997. Triggering basaltic volcanic eruptions by bubble-
1015 melt separation. *Nature* 385, 518-20.
1016
1017
1018